

Spin-Orbital Hallmarks of Unconventional Superconductors Without Inversion Symmetry

Yuri Fukaya,¹ Shun Tamura,¹ Keiji Yada,¹ Yukio Tanaka,¹ Paola Gentile,² and Mario Cuoco²

¹*Department of Applied Physics, Nagoya University, Nagoya 464-8603, Japan*

²*CNR-SPIN, I-84084 Fisciano (Salerno), Italy, c/o Università di Salerno, I-84084 Fisciano (Salerno), Italy*

The spin-orbital polarization of superconducting excitations in momentum space is shown to provide distinctive marks of unconventional pairing in the presence of inversion symmetry breaking. Taking the prototypical example of an electronic system with atomic spin-orbit and orbital-Rashba couplings, we provide a general description of the spin-orbital textures and their most striking changeover moving from the normal to the superconducting state. We find that the variation of the spin-texture is strongly imprinted by the combination of the misalignment of spin-triplet \mathbf{d} -vector with the inversion asymmetry \mathbf{g} -vector coupling and the occurrence of superconducting nodal excitations. Remarkably, the multi-orbital character of the superconducting state allows to unveil a unique type of topological transition for the spin-winding around the nodal points. This finding indicates the fundamental topological relation between chiral and spin-winding in nodal superconductors. By analogy between spin- and orbital-triplet pairing we point out how orbital polarization patterns can be also employed to assess the character of the superconducting state.

Introduction. — The Rashba spin-orbit (SO) coupling [1, 2] is the manifestation of a fundamental relativistic effect due to structural inversion symmetry breaking (ISB) that leads to spin-momentum locking with lifting of spin degeneracy and remarkable phenomena such as non-standard magnetic textures [3, 4], spin Hall [5] and topological spin Hall [6], Edelstein effects [7], etc. [8].

Recently, it has been realized that spin-momentum locking can also occur from the ISB driven orbital polarization of electrons in solids which is, then, linked with the spin-sector by the atomic SO coupling. The role of spin and orbital polarization in materials has built a different view of the manifestation of ISB with respect to the conventional spin-Rashba effect, leading to the so-called orbital-driven Rashba coupling [9]. The orbital Rashba (OR) effect can yield chiral orbital textures and orbital dependent spin-vector via the SO coupling [9–15]. Evidences of anomalous energy splitting and of a key role played by the orbital degree of freedom have been demonstrated on a large variety of surfaces, i.e. Au(111), Pb/Ag(111) [16], Bi/Ag(111) [17], etc. as well as in transition metal oxides based interfaces, i.e. LaAlO₃-SrTiO₃ [18, 19].

In superconductors without inversion symmetry [20, 21] the presence of non-degenerate spin- and orbital polarized electronic states is generally expected to lead to unconventional pairing, with the occurrence of spin-triplet order parameters and singlet-triplet spin mixing [22–24], non-standard surface states [25, 26], as well as topological phases [27–35].

Experimental direct probes by using angle- and spin-orbital resolved photoemission spectroscopy in the normal [36–39] and superconducting (SC) phase [40] can be extremely useful for establishing the nature of the SC state and the underlying degree of spin-orbital entanglement or the occurrence of competing orders. Along this line it would be highly desirable to have distinctive de-

tectable signatures associated with the spin-orbital polarizations to single out the nature of the SC phase. Symmetry plays a relevant role in such identification. For instance, skyrmionic patterns in the Brillouin zone (BZ) have been suggested as marks to make the topological order more accessible in ferromagnetic semiconductor/*s*-wave superconductor heterostructure assuming that both time- and inversion-symmetry are broken [41]. On the other hand, the fundamental interrelation between chiral spin-orbital textures in reciprocal space and unconventional pairing solely due to ISB has not been yet fully established.

In this Letter we focus on the class of low-dimensional superconductors with time-reversal (TR) and broken inversion symmetry. The aim is to assess how the spin-orbital texture of the SC excitations can unveil the nature of the SC state and, eventually, its topological character. We show that the spin-polarization pattern is generally imprinted by the relative alignment of spin-triplet \mathbf{d} -vector with the inversion asymmetry \mathbf{g} -vector coupling. A fundamental issue emerges in nodal topological superconductors when considering the occurrence of spin-winding around the nodal points. To face this problem on a general ground we employ a prototypical electronic system with atomic SO and orbital-Rashba coupling, whose spin-orbital textures can manifest deviations from the typical ones due to the spin-Rashba coupling and can manifest topological SC phases with orbital-driven pairing. We find that at the nodal points topological transitions for the spin-winding can occur due to the emergence of vanishing spin amplitude lines connecting the nodal points. This outcome sets the fundamental interplay between chiral and spin- or orbital winding in nodal superconductors with ISB.

Topological spin-texture: single orbital model description. — We start by introducing a minimal model that can describe the spin-texture of the SC state due to

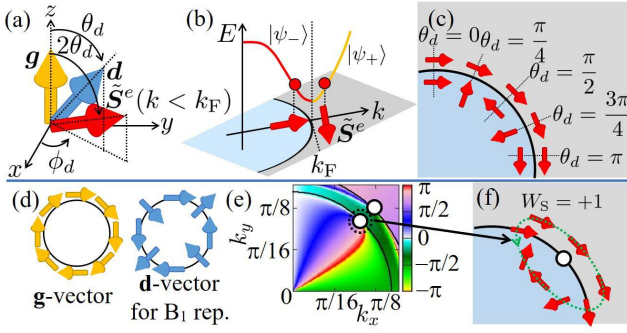


FIG. 1. (a) Schematic spin-space representation of the relative orientations among the ISB \mathbf{g} -vector, the spin-triplet pairing \mathbf{d} -vector, and the spin direction corresponding to an excited state for $k < k_F$, with k_F being the Fermi wave vector. θ_d is the polar angle between \mathbf{g} - and \mathbf{d} -vector and ϕ_d is the angle of the spin vector measured with respect to the in-plane x direction. (b) Sketch of the energy dispersion along a given direction and of the spin orientation for excited states at given momentum larger (electron-like) and smaller (hole-like) than the Fermi vector in the SC state. $|\psi_+\rangle$ ($|\psi_-\rangle$) corresponds to the eigenstate for $k \geq k_F$ ($k < k_F$). Here, $\hat{\mathbf{S}}^e$ for $k \geq k_F$ is collinear to \mathbf{g} . (c) Spin orientations of the excited states above and below the Fermi level at $\theta_d = 0, \pi/4, \pi/2, 3\pi/4$, and π . (d) Orientation of the \mathbf{g} -vector and spin-vector for a Rashba-type spin-momentum coupling, and \mathbf{d} -vector orientation for the B_1 representation of the point group C_{4v} on the Fermi surface (black solid line). (e) Orientation of electron component of the spin-polarization for the first excited state of the B_1 phase in the single-band model at $\Lambda/t = 8.0 \times 10^{-2}$ and $\mu/t = 0.25$. Black solid line indicates the Fermi surface in the normal state and white circle is for the position of the nodal point. (f) Schematic illustration of the winding spin-texture of (e) around the point node with spin-winding number $W_S = +1$.

the interplay of inversion asymmetric SO coupling and spin-triplet pairing. Due to ISB the pairing has mixture of spin-triplet and singlet components. Since the spin-singlet pairing does not affect the spin-texture, the central focus is on the consequences of the spin-triplet pair potential. Let us then consider a physical scenario where the SC state is described by a \mathbf{d} -vector for the spin-triplet Cooper pairs with a generic orientation, compatible with the crystal symmetry, with respect to the \mathbf{g} -vector setting the spin-momentum locking of the electronic states [Fig. 1(a)]. Then, the electronic description can be expressed by the following Hamiltonian:

$$\hat{H}_{\text{BdG}} = \begin{pmatrix} -\mu\hat{\sigma}_0 + \hat{h}(\mathbf{k}) & \hat{\Delta}(\mathbf{k}) \\ \hat{\Delta}^\dagger(\mathbf{k}) & \mu\hat{\sigma}_0 - \hat{h}^t(-\mathbf{k}) \end{pmatrix}, \quad (1)$$

where μ and $\hat{\Delta}(\mathbf{k}) = i\hat{\sigma}_y[\psi + \hat{\boldsymbol{\sigma}} \cdot \mathbf{d}(\mathbf{k})]$ denote the chemical potential, and the singlet (ψ) and triplet order parameters (\mathbf{d}), and \hat{h} is the normal state term

$$\hat{h}(\mathbf{k}) = \varepsilon(\mathbf{k})\hat{\sigma}_0 + \Lambda\mathbf{g}(\mathbf{k}) \cdot \hat{\boldsymbol{\sigma}}, \quad (2)$$

$$\mathbf{g}(\mathbf{k}) = (g_x(\mathbf{k}), g_y(\mathbf{k}), g_z(\mathbf{k})), \quad (3)$$

with $\varepsilon(\mathbf{k})$ and \mathbf{g} being the kinetic energy and inversion asymmetry coupling, while Λ denotes the strength of the ISB potential, and $\hat{\sigma}_i$ ($i = 0, x, y, z$) are the Pauli matrices in spin space. Here, the \mathbf{d} -vector has the usual matrix form in terms of the components associated with the spin-triplet configurations as $\Delta_{\uparrow,\uparrow} - \Delta_{\downarrow,\downarrow} = -2d_x(\mathbf{k})$, $\Delta_{\uparrow,\uparrow} + \Delta_{\downarrow,\downarrow} = 2id_y(\mathbf{k})$, and $\Delta_{\uparrow,\downarrow} + \Delta_{\downarrow,\uparrow} = 2d_z(\mathbf{k})$. If the \mathbf{d} - and \mathbf{g} -vectors are misaligned by an angle θ_d [Fig. 1(a)], then the electron spin orientation corresponding to the excitations close to the Fermi level (k_F) will manifest a distinctive pattern [Fig. 1(b)]. Indeed, by means of perturbation theory, we can show (see Supplemental Material [42]) that for $k \geq k_F$ the spin orientation is collinear to the \mathbf{g} -vector while it gets rotated by an angle $2\theta_d$ for $k < k_F$. Hence, a variation of the mismatch angle between \mathbf{d} - and \mathbf{g} -vectors along the Fermi surface can lead to a spin-texture with a general trend that is marked by an asymmetric angular dependence in the electron- and hole-branch of the low energy excitation [Fig. 1(c)]. Taking into account the configuration in Fig. 1(a), one can generally demonstrate [42] that the spin orientation for the excited state $|\psi_+\rangle$ at $k \geq k_F$ is collinear to the \mathbf{g} -vector, while for $|\psi_-\rangle$ at $k < k_F$ it depends on the angles θ_d and ϕ_d . Indeed, if we define $\hat{s}_{-\gamma}^e \equiv \langle \psi_- | \hat{S}_\gamma^e | \psi_- \rangle$ with $\gamma = x, y, z$, the spin-vector for $k < k_F$ is given by $[\hat{s}_{-x}^e, \hat{s}_{-y}^e, \hat{s}_{-z}^e] \sim [a_s \cos \phi_d \sin 2\theta_d, a_s \sin \phi_d \sin 2\theta_d, a_s \cos 2\theta_d]$, where $\hat{S}_{i=x,y,z}^e$ is the electron component of the spin operator $\hat{S}_i^e = \frac{1}{2}[1 + \hat{\tau}_3] \otimes \hat{S}_i$ by projection via the particle-hole operator $\hat{\tau}_3$, and a_s is an amplitude depending on the energy distance of the excited state from the Fermi level and the strength of the superconducting pairing [42]. It is then immediate to deduce that the spin orientation is collinear to \mathbf{g} with $\theta_d = 0$ while for perpendicularly oriented \mathbf{g} - and \mathbf{d} -vectors, i.e. $\theta_d = \pi/2$, the spin polarization is anti-parallel to \mathbf{g} . In general, we obtain that the spin polarization lies in the same plane of \mathbf{g} and \mathbf{d} and it deviates of an angle $2\theta_d$ from \mathbf{g} .

We confirm such behavior by explicitly determining the spin-polarization for various spin-triplet pairing states. Then we look for the spin-windings in the xy -plane. In order to obtain the spin-vector in the xy -plane, that is, $\langle \psi_\pm | \hat{S}_z^e | \psi_\pm \rangle = 0$, both \mathbf{d} - and \mathbf{g} -vectors are in the xy -plane. Indeed, when computing the spin-texture for a Rashba-type \mathbf{g} -vector and a \mathbf{d} -vector belonging to the B_1 representation of the C_{4v} point group that are given by $\mathbf{g} = (-\sin(k_y), \sin(k_x), 0)$ and $\mathbf{d} = (\sin(k_y), \sin(k_x), 0)$ [Fig. 1(d)], we obtain the orientation of the spin-polarization [Fig. 1(e)] in the BZ and there is a two-dimensional spin-winding around the nodal points along the diagonal of the BZ [Fig. 1(f)]. Here, we define the spin-winding number as $W_S = \frac{1}{2\pi} \oint_C d\theta_S^{\text{SC1}}(\mathbf{k})$ with the integral route C and the direction of spin-texture $\theta_S^{\text{SC1}}(\mathbf{k}) = \arg[\langle \psi_{+(-)} | \hat{S}_x^e | \psi_{+(-)} \rangle + i \langle \psi_{+(-)} | \hat{S}_y^e | \psi_{+(-)} \rangle]$ for $k \geq k_F$ ($k < k_F$). Due to the angular relation of \mathbf{d} -

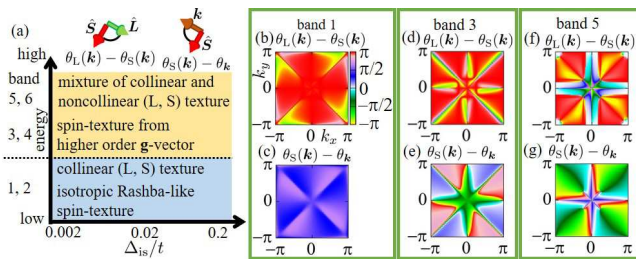


FIG. 2. (a) Schematic description of the spin-orbital texture for the three-orbital model in the normal state as a function of the band index, from lowest to the highest occupied, and in terms of the OR (Δ_{is}) and atomic spin-orbit ($\lambda_{\text{SO}}/t = 0.10$) couplings. $\theta_S(\mathbf{k})$, $\theta_L(\mathbf{k})$, $\theta_{\mathbf{k}}$ denote the angle of the spin-, orbital- vectors and momentum \mathbf{k} measured with respect to the x -axis. (b),(f),(h) denote the relative angle between the spin and orbital polarization for the bands 1,3,5. (c),(g),(i) indicate the relative angle between the spin orientation and the momentum within the BZ. The lowest occupied bands (i.e. 1,2) exhibit a Rashba-type spin-momentum locking. The remaining bands are marked by spin-textures with higher than the linear order in the effective \mathbf{g} -vector coupling and with a mixing of collinear and noncollinear configurations for the \mathbf{L} and \mathbf{S} angular momentum. We report only the spin-orbital pattern for the bands 1,3,5 because the others are linked to these by TR symmetry.

and \mathbf{g} -vectors at each \mathbf{k} point as shown in Fig. 1(c), the spin polarization can wind around the nodal point with $W_S = +1$ [Fig. 1(f)]. We note that the spin-polarization also winds around the high symmetry points in the BZ. At this stage, it is relevant to ask whether the spin-winding always occurs around the nodal points. By generalizing the single-band model to include higher order terms in the inversion asymmetric coupling of the type $(\sin k)^3$ or $(\sin k)^5$, we find that the spin-winding is robust and it is not affected by the modification of the \mathbf{g} -vector [42]. Likewise, we also obtain the spin-windings for the B_2 representation with nodal points on the x and y -axis.

Spin-orbital texture in multi-orbital electronic systems.

— In order to deepen the relation between spin-winding and nodal excitations beyond the single orbital description, we consider a multi-orbital model that includes both an OR term and the atomic SO coupling. The model Hamiltonian in the normal state [43] can be generally expressed in the basis $[|\uparrow, \downarrow\rangle \otimes (d_{yz}, d_{zx}, d_{xy})]$ as:

$$\hat{H}(\mathbf{k}) = \hat{\sigma}_0 \otimes [f_x(\mathbf{k})\hat{L}_x^2 + f_y(\mathbf{k})\hat{L}_y^2 + f_z(\mathbf{k})\hat{L}_z^2] + \lambda_{\text{SO}}\hat{\sigma} \cdot \hat{L} + \Delta_{\text{is}}\hat{\sigma}_0 \otimes [g_x(\mathbf{k})\hat{L}_x + g_y(\mathbf{k})\hat{L}_y], \quad (4)$$

with $f_x(\mathbf{k}) = \frac{1}{2}[-\varepsilon_{yz}(\mathbf{k}) + \varepsilon_{zx}(\mathbf{k}) + \varepsilon_{xy}(\mathbf{k})]$, while the other components are obtained by permuting the (x, y, z) indices, and $\varepsilon_{yz}(\mathbf{k}) = 2t_1(1 - \cos k_y) + 2t_3(1 - \cos k_x)$, $\varepsilon_{zx} = \varepsilon_{yz}(y \rightarrow x)$, $\varepsilon_{xy}(\mathbf{k}) = 4t_2 - 2t_2(\cos k_x + \cos k_y) + \Delta_t$. Here, $\hat{\sigma}$ and \hat{L} are matrices associated with spin 1/2 and the effective $L = 1$ orbital angular momentum in the

projected (d_{yz}, d_{zx}, d_{xy}) sector. We consider representative hopping amplitudes, i.e. $t_1 = t = 0.10$, $t_2 = t$, and $t_3 = 0.10t$ and $\Delta_t/t = -0.50$ for the crystal field potential, which are typical values encountered in the atomistic description of the electronic structure of $3d$ -bands in oxides. A modification of the electronic amplitudes does not qualitatively alter our conclusions. Then, in order to evaluate the changeover of the spin-orbital texture we fix $\lambda_{\text{SO}}/t = 0.10$ and vary Δ_{is}/t [Fig. 2(a)] so to tune the hierarchy of the two SO interactions. The character of the spin- and orbital polarized states within the BZ depends on which bands are taken at the Fermi level. In Fig. 2, we summarize the two main features of the spin-orbital textures concerning both the interrelation between the spin and orbital orientations and the spin- or orbital momentum locking. Firstly, due to the symmetry of the model Hamiltonian, the ISB leads to planar nonvanishing spin and orbital polarizations at any given \mathbf{k} except for the high symmetry points [42] with a relative angle, $\theta_L(\mathbf{k}) - \theta_S(\mathbf{k})$, that is about uniformly collinear in the BZ for the lowest occupied bands (i.e. 1,2) [Fig. 2(b)]. Here, $\theta_S(\mathbf{k})$ ($\theta_L(\mathbf{k})$) stands for the orientation of spin- (orbital) vector. The highest energy bands (i.e. 3,4,5,6), instead, exhibit a more intricate structure. Indeed, the spin and orbital polarizations are not anymore collinear near the high symmetry lines [Fig. 2(d)(f)]. Such behavior is also encountered in the relative orientation of the spin polarization with respect to the direction of the momentum \mathbf{k} set by the angle $\theta_{\mathbf{k}}$. The spin is perpendicular to the momentum (i.e. $\theta_S(\mathbf{k}) - \theta_{\mathbf{k}} \sim \pm\pi/2$) only for the lowest occupied bands (i.e. 1,2) [Fig. 2(c)]. On the contrary, the remaining electronic states exhibit a non-isotropic spin-momentum pattern that can be accounted by the presence of higher than linear order in the direct \mathbf{g} -vector spin-momentum coupling [Fig. 2(e)(g)]. This is a general behavior which is characteristic of the interplay between the OR and the atomic SO coupling.

Topological spin-winding in nodal topological superconductors. — We evaluate how the spin-texture changes in the SC state by focusing on the occurrence and evolution of spin-winding numbers W_S around the nodal points. Such feature sets the most striking changeover from the normal to the superconducting phase because the normal state does not exhibit local spin-winding close to the point nodes position. To do that we consider an inter-orbital spin-triplet/orbital-singlet/ s -wave SC state belonging to the B_1 representation of the C_{4v} point group symmetry [44]. The spin-winding can be defined because the z -component of the spin-texture is zero for this B_1 representation. Such configuration is well suited for our purposes because it is known [44] to be energetically favorable in a wide range of parameters and that, for this symmetry channel, the superconductor is topologically nontrivial exhibiting nodal points along the diagonal of the BZ [Fig. 3(a)]. Then, to single out the changeover of the SC spin-texture from that in the normal state we

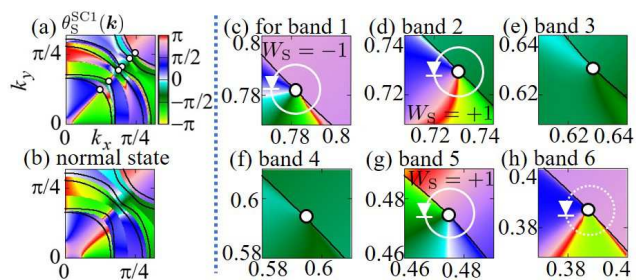


FIG. 3. Spin-texture of the lowest excited states corresponding to the inter-orbital B_1 superconducting phase (a) and corresponding spin-pattern in the normal state including the hole branch (b) at $\Delta_{is}/t = 0.20$ and $\lambda_{SO}/t = 0.10$. White circle indicates the nodal points. From (c) to (h) we zoom on the spin-texture of the superconducting excitations around the nodal points for the corresponding bands at the Fermi level from the lowest to the highest energy. The bands 1,2 and 5 exhibit spin-winding numbers around the nodal points ($W_S = \pm 1$) while the excitations associated with the bands 3 and 4 have uniform spin orientation ($W_S = 0$), and, finally, the band 6 has an incomplete winding around the point node thus $W_S = 0$.

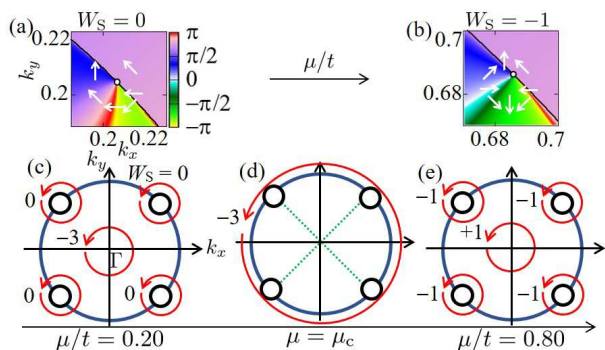


FIG. 4. (a)-(b) Demonstration of topological transition of spin-winding numbers for the band 6 as a function of the chemical potential for a representative excitation branch around the nodal point. Small circle denotes the nodal point. (c)-(e) schematically indicate the global rearrangement of the spin-winding numbers W_S with the occurrence at the critical amplitude of the chemical potential (μ_c) of lines of zero spin-amplitude (green dotted line) connecting the TR corresponding nodal points. The sum of the spin-winding numbers around the nodal points and the center of the BZ is conserved from (c) to (e).

determine both patterns as reported in Fig. 3(b). Remarkably, its investigation for the multi-orbital topological superconductor reveals that the spin-winding is not tied to the nodal point. Indeed, for a representative set of parameters, we demonstrate that not all the excitations around the nodal position manifest a spin-winding.

The lowest occupied bands which are well described by an effective single-band model with Rashba-type SO coupling [42] have the same spin-winding numbers as those in the single-orbital model [Fig. 3(c)-(d)]. On the

other hand, the highest occupied bands which mainly arise from the (d_{yz}, d_{zx})-orbitals and more significantly deviate from a Rashba-type spin-momentum locking, can be employed to prove the complex topological structure of the spin-winding in the BZ [Fig. 3(e)-(h)]. The obtained results clarify a fundamental question on the way the spin-winding around the nodal points can vary undergoing a topological transition and, in turn, affect the overall spin-pattern of the excitations. We point out that, if the superconductor manifests a Lifshitz-type electronic transition by merging the nodal points having opposite chiral winding numbers due to the chiral symmetry owed by the SC Hamiltonian [32–34, 44], then these two nodal points have opposite spin-winding numbers and the spin-winding is also expected to disappear due to nodes annihilation and gap formation in the spectrum. On the other hand, it is less obvious to obtain a change of the spin-winding number without any topological modification of the nodal electronic spectrum. Hence, the investigated multi-orbital superconductor allowed to uncover a novel path for topological transition of the spin-winding. For the band 6 corresponding to the highest occupied one, as we demonstrate in Fig. 4, the spin-winding numbers for a given branch of the excitation spectra can be removed by tuning the chemical potential [see Figs. 4(a)-(b)] and the transition occurs when a configuration with zero spin amplitude can be obtained in the excitation states [Fig. 4(d)]. This type of local topological transition is basically accompanied by a global change of the topological spin-winding numbers as sketched in Fig. 4 (d). The presence of multi-orbital components in the superconductor is a fundamental requisite to achieve a quenching of the spin-momentum amplitude due to contributions of inequivalent orbital states. We point out that the orbital texture, due to the orbital singlet nature of the superconducting state, does not exhibit any orbital winding around the nodal point. Although the analysis is focused on the role of spin-triplet pairing, by analogy one would get similar signatures when considering orbital-triplet with spin-singlet configurations.

Conclusions. — We demonstrated that the spin-orbital texture of non-centrosymmetric superconductors with TR symmetry can unveil fundamental aspects of the pairing state. A mismatch of the spin (orbital) polarizations from the normal to the superconducting state can set the hallmarks of the presence of non-trivial spin- (orbital) triplet vectors. Remarkably, for pairing configurations having nodal excitations we expect to observe a local spin- (or orbital) winding which can undergo topological transitions without any change in the electronic spectrum. Such behavior is fundamentally tied to the degree of spin-orbital entanglement of the SC state and to a spin-momentum coupling which deviates from the Rashba-type. Our findings are experimentally accessible due to the recent advancements of the application of circularly-polarized spin- and angle-resolved photoemis-

sion spectroscopy. Indeed, the combination of orbital-selectivity of circularly polarized light with spin detection can allow for direct and independent access to the spin- and orbital vectors throughout the BZ and consequently assess the unconventional nature of low-dimensional non-centrosymmetric SC states.

This work was supported by the JSPS Core-to-Core program ‘‘Oxide Superspin’’ international network, and a JSPS KAKENHI (Grants Nos. JP15H05851, JP15H05853, JP15K21717, JP18H01176, and JP18K03538), and the project Quantox of QuantERA-NET Cofund in Quantum Technologies, implemented within the EU-H2020 Programme.

-
- [1] E. I. Rashba, *Sov. Phys. - Solid State* **2**, 1109 (1960).
 [2] Y. A. Bychkov and E. I. Rashba, *JETP. Lett.* **39**, 78 (1984).
 [3] I. E. Dzyaloshinskii, *J. Exp. Theor. Phys.* **5**, 1259 (1957).
 [4] T. Moriya, *Phys. Rev.* **120**, 91 (1960).
 [5] J. Sinova, D. Culcer, Q. Niu, N. A. Sinitsyn, T. Jungwirth, and A. H. MacDonald, *Phys. Rev. Lett.* **92**, 126603 (2004).
 [6] C.-Z. Chang, J. Zhang, X. Feng, J. Shen, Z. Zhang, M. Guo, K. Li, Y. Ou, P. Wei, L.-L. Wang, Z.-Q. Ji, Y. Feng, S. Ji, X. Chen, J. Jia, X. Dai, Z. Fang, S.-C. Zhang, K. He, Y. Wang, L. Lu, X.-C. Ma, and Q.-K. Xue, *Science* **340**, 167 (2013).
 [7] V. M. Edelstein, *Solid State Communications* **73**, 233 (1990).
 [8] A. Manchon, H. C. Koo, J. Nitta, and R. A. Duine, *Nat. Mat.* **14**, 871 (2015).
 [9] S. R. Park, C. H. Kim, J. Yu, J. H. Han, and C. Kim, *Phys. Rev. Lett.* **107**, 156803 (2011).
 [10] J.-H. Park, C. H. Kim, H.-W. Lee, and J. H. Han, *Phys. Rev. B* **87**, 041301(R) (2013).
 [11] P. Kim, K. T. Kang, G. Go, and J. H. Han, *Phys. Rev. B* **90**, 205423 (2014).
 [12] J. Hong, J.-W. Rhim, C. Kim, S. R. Park, and J.-H. Shim, *Sci. Rep.* **5**, 13488 (2015).
 [13] B. Kim, C. H. Kim, P. Kim, W. Jung, Y. Kim, Y. Koh, M. Arita, K. Shimada, H. Namatame, M. Taniguchi, J. Yu, and C. Kim, *Phys. Rev. B* **85**, 195402 (2012).
 [14] J.-H. Park, C. H. Kim, J.-W. Rhim, and J. H. Han, *Phys. Rev. B* **85**, 195401 (2012).
 [15] S. R. Park, J. Han, C. Kim, Y. Y. Koh, C. Kim, H. Lee, H. J. Choi, J. H. Han, K. D. Lee, N. J. Hur, M. Arita, K. Shimada, H. Namatame, and M. Taniguchi, *Phys. Rev. Lett.* **108**, 046805 (2012).
 [16] L. El-Kareh, G. Buchter, H. Bentmann, S. Blügel, F. Reinert, and M. Bode, *New J. Phys.* **16**, 045017 (2014).
 [17] S. Schirone, E. E. Krasovskii, G. Bihlmayer, R. Piquerel, P. Gambardella, and A. Mugarza, *Phys. Rev. Lett.* **114**, 166801 (2015).
 [18] P. D. C. King, S. McKeown Walker, A. Tamai, A. de la Torre, T. Eknapakul, P. Buaphet, S.-K. Mo, W. Meevasana, M.S. Bahramy, and F. Baumberger, *Nat. Commun.* **5**, 3414 (2014).
 [19] H. Nakamura, T. Koga, and T. Kimura *Phys. Rev. Lett.* **108**, 206601 (2012).
 [20] E. Bauer and M. Sigrist, *Non-Centrosymmetric Superconductors: Introduction and Overview*, vol. **847**, Lecture Notes in Physics (Springer, 2012).
 [21] M. Smidman, M. B. Salamon, H. Q. Yuan, and D. F. Agterberg, *Report of Progress in Physics* **80**, 036501 (2017).
 [22] L. P. Gorkov and E. I. Rashba, *Phys. Rev. Lett.* **87**, 037004 (2001).
 [23] P. A. Frigeri, D. F. Agterberg, A. Koga, and M. Sigrist, *Phys. Rev. Lett.* **92**, 097001 (2004).
 [24] K. Yada, S. Onari, Y. Tanaka, and J.I. Inoue, *Phys. Rev. B* **80**, 140509(R) (2009).
 [25] C. K. Lu and S. Yip, *Phys. Rev. B* **78**, 132502 (2008).
 [26] A. B. Vorontsov, I. Vekhter, and M. Eschrig, *Phys. Rev. Lett.* **101**, 127003 (2008).
 [27] M. S. Scheurer and J. Schmalian, *Nat. Commun.* **6**, 6005 (2015).
 [28] Y. Tanaka, T. Yokoyama, A. V. Balatsky, and N. Nagaosa, *Phys. Rev. B* **79**, 060505(R) (2009).
 [29] M. Sato and S. Fujimoto, *Phys. Rev. B* **79**, 094504 (2009).
 [30] A. P. Schnyder, P. M. R. Brydon, D. Manske, and C. Timm, *Phys. Rev. B* **82**, 184508 (2010).
 [31] Y. Tanaka, Y. Mizuno, T. Yokoyama, K. Yada, and M. Sato, *Phys. Rev. Lett.* **105**, 097002 (2010).
 [32] K. Yada, M. Sato, Y. Tanaka, and T. Yokoyama, *Phys. Rev. B* **83**, 064505 (2011).
 [33] M. Sato, Y. Tanaka, K. Yada, and T. Yokoyama, *Phys. Rev. B* **83**, 224511 (2011).
 [34] P. M. R. Brydon, A. P. Schnyder, and C. Timm, *Phys. Rev. B* **84**, 020501(R) (2011).
 [35] Z.-J. Ying, M. Cuoco, C. Ortix, and P. Gentile, *Phys. Rev. B* **96**, 100506(R) (2017).
 [36] S. Borisenko, D. Evtushinsky, I. Morozov, S. Wurmehl, B. Büchner, A. Yaresko, T. Kim, M. Hoesch, T. Wolf, and N. Zhigadlo, *Nat. Phys.* **12**, 311 (2016).
 [37] P. D. Johnson, H.-B. Yang, J. D. Rameau, G. D. Gu, Z.-H. Pan, T. Valla, M. Weinert, A. V. Fedorov, *Phys. Rev. Lett.* **114**, 167001 (2015).
 [38] S.-L. Wu, K. Sumida, K. Miyamoto, K. Taguchi, T. Yoshikawa, A. Kimura, Y. Ueda, M. Arita, M. Nagao, S. Watauchi, I. Tanaka, and T. Okuda, *Nat. Comm.* **8**, 1919, (2017).
 [39] R. P. Day, G. Levy, M. Michiardi, B. Zwartsenberg, M. Zonno, F. Ji, E. Razzoli, F. Boschini, S. Chi, R. Liang, P. K. Das, I. Vobornik, J. Fujii, W. N. Hardy, D. A. Bonn, I. S. Elfimov, and A. Damascelli, *Phys. Rev. Lett.* **121**, 076401 (2018).
 [40] M. Neupane, N. Alidoust, M. M. Hosen, J.-X. Zhu, K. Dimitri, S.-Y. Xu, N. Dhakal, R. Sankar, I. Belopolski, D. S. Sanchez, T.-R. Chang, H.-T. Jeng, M. Z. Hasan, and T. Durakiewicz, *Nat. Commun.* **7**, 13315 (2016).
 [41] K. Björnson and A. M. Black-Schaffer, *Phys. Rev. B* **89**, 134518 (2014).
 [42] In the Supplemental Material we provide the details of the derivation via perturbation theory of the general orientation of the spin-polarization of the lowest energy excitation in the superconducting state in terms of the relative alignment between the \mathbf{d} -vector and the \mathbf{g} -vector. Furthermore, we present the spin-texture for the single-orbital model with spin-triplet pairing and cubic or fifth order terms in the spin-momentum coupling. Finally, we derive the single-orbital Rashba-type model from the multi-orbital electronic model including the atomic spin-

orbit and orbital Rashba couplings.

- [43] G. Khalsa, B. Lee, and A. H. MacDonald, Phys. Rev. B **88**, 041302(R) (2013).
- [44] Y. Fukaya, S. Tamura, K. Yada, Y. Tanaka, P. Gentile, and M. Cuoco, Phys. Rev. B **97**, 174522 (2018).

Supplemental Material: “Spin-Orbital Hallmarks of Unconventional Superconductors Without Inversion Symmetry”

Yuri Fukaya,¹ Shun Tamura,¹ Keiji Yada,¹ Yukio Tanaka,¹ Paola Gentile,² and Mario Cuoco²

¹*Department of Applied Physics, Nagoya University, Nagoya 464-8603, Japan*

²*CNR-SPIN, I-84084 Fisciano (Salerno), Italy, c/o Università di Salerno, I-84084 Fisciano (Salerno), Italy*

In the Supplemental Material we provide the details of the determination via perturbation theory of the general orientation of the spin-polarization for the lowest energy excitations in the superconducting state in terms of the relative alignment between the spin-triplet \mathbf{d} -vector and the inversion asymmetry \mathbf{g} -vector coupling. Furthermore, we derive the single-orbital Rashba-type description from the multi-orbital electronic model including the atomic spin-orbit and orbital Rashba couplings. Finally, we determine the spin-texture for the single-orbital model with spin-triplet pairing and cubic or fifth order terms in the spin-momentum coupling to assess the robustness of the spin-winding around the nodal points of the superconducting spectrum.

I. SPIN POLARIZATION BY PERTURBATION THEORY IN THE SINGLE ORBITAL MODEL WITH SPIN-TRIPLET PAIRING AND INVERSION SYMMETRY BREAKING

We investigate the electron component of the spin polarization of the superconducting excited states assuming a single-orbital model in the presence of an inversion asymmetric potential. The analysis is performed by means of perturbation theory. In the normal state, the Hamiltonian with the inversion symmetry breaking along the z -direction is given by

$$\hat{h}(\mathbf{k}) = \varepsilon(\mathbf{k})\hat{\sigma}_0 + \Lambda\mathbf{g} \cdot \hat{\boldsymbol{\sigma}}, \quad (1)$$

$$\mathbf{g}(\mathbf{k}) = (g_x(\mathbf{k}), g_y(\mathbf{k}), g_z(\mathbf{k})). \quad (2)$$

Here, $\varepsilon(\mathbf{k})$ and $\mathbf{g}(\mathbf{k})$ denote the kinetic energy of the electron and the inversion asymmetric \mathbf{g} -vector coupling whose strength is Λ . Moreover, $\hat{\sigma}_i$ ($i = 0, x, y, z$) are the Pauli matrices in spin space.

We determine the spin polarization components by evaluating the expectation values of the related spin operators. In the normal state, we assume that \mathbf{g} -vector lies on xy -plane and $g_z(\mathbf{k}) = 0$. Then, the eigenvalues and the corresponding eigenstates of the Hamiltonian are given by

$$E_{\pm} = \varepsilon(\mathbf{k}) \pm \Lambda\sqrt{g_x^2(\mathbf{k}) + g_y^2(\mathbf{k})},$$

$$|+\rangle = \begin{pmatrix} \cos \frac{\theta}{2} \\ e^{i\phi} \sin \frac{\theta}{2} \end{pmatrix}, \quad |-\rangle = \begin{pmatrix} -e^{-i\phi} \sin \frac{\theta}{2} \\ \cos \frac{\theta}{2} \end{pmatrix},$$

with $\theta = \pi/2$, $\cos \phi = g_x(\mathbf{k})/\sqrt{g_x^2(\mathbf{k}) + g_y^2(\mathbf{k})}$, and $\sin \phi = g_y(\mathbf{k})/\sqrt{g_x^2(\mathbf{k}) + g_y^2(\mathbf{k})}$. It is immediate to verify that the expectation values of the spin operators are

given by

$$\langle \pm | \hat{S}_x | \pm \rangle = \pm \frac{g_x(\mathbf{k})}{\sqrt{g_x^2(\mathbf{k}) + g_y^2(\mathbf{k})}},$$

$$\langle \pm | \hat{S}_y | \pm \rangle = \pm \frac{g_y(\mathbf{k})}{\sqrt{g_x^2(\mathbf{k}) + g_y^2(\mathbf{k})}},$$

$$\langle \pm | \hat{S}_z | \pm \rangle = 0,$$

where $\hat{S}_{i=x,y,z}$ are the spin operators expressed in terms of the Pauli matrices. Thus, the z -component of the spin operator is zero (except that at the high symmetry points) and the in-plane x and y -components are generally non-vanishing. The planar structure of the spin polarization is a general consequence of the symmetry property of the model Hamiltonian. If the transformation $\hat{S}_z \rightarrow -\hat{S}_z$ is a symmetry for the quantum system upon examination, then, due the absence of degeneracy at any (k_x, k_y) different from the time reversal invariant momenta, the expectation value of the z -component of the spin operator is identically zero. Thus, one can focus the analysis only on the spin orientation in the xy -plane.

In the superconducting state we consider the Bogoliubov-de Gennes (BdG) Hamiltonian constructed from $\hat{h}(\mathbf{k})$ and including both spin-singlet and triplet pairings as follows

$$\hat{H}_{\text{BdG}}(\mathbf{k}) = \begin{pmatrix} -\mu\hat{\sigma}_0 + \hat{h}(\mathbf{k}) & \hat{\Delta}(\mathbf{k}) \\ \hat{\Delta}^\dagger(\mathbf{k}) & \mu\hat{\sigma}_0 - \hat{h}^t(-\mathbf{k}) \end{pmatrix}, \quad (3)$$

$$\hat{\Delta}(\mathbf{k}) = i\sigma_y[\psi(\mathbf{k}) + \hat{\boldsymbol{\sigma}} \cdot \mathbf{d}(\mathbf{k})], \quad (4)$$

with the chemical potential μ . Here, for convenience and clarity of computation we assume that \mathbf{g} has a generic orientation in the spin-space, $\hat{\Delta}(\mathbf{k})$ denotes the gap function, with $\psi(\mathbf{k})$ being the spin-singlet pairing, and $\mathbf{d}(\mathbf{k})$ the spin-triplet order parameter. Starting from this BdG Hamiltonian, one can introduce the electron component of the spin polarization within the xy -plane for the m -th excited state of the superconducting spectrum by means of the following relation

$$\theta_S^{\text{SC}m} = \arg[\langle \Psi_m | \tilde{S}_x^e | \Psi_m \rangle + i\langle \Psi_m | \tilde{S}_y^e | \Psi_m \rangle], \quad (5)$$

where $|\Psi_m\rangle$ is the m -th eigenstate of the spectrum of the BdG Hamiltonian and $\hat{S}_{i=x,y,z}^e$ are the spin operators projected onto the electron space:

$$\tilde{S}_i^e = \frac{1}{2}[1 + \hat{\tau}_3] \otimes \hat{S}_i, \quad (6)$$

$$\hat{\tau}_3 = \begin{pmatrix} 1 & 0 \\ 0 & -1 \end{pmatrix}, \quad (7)$$

with the Pauli matrix $\hat{\tau}_3$ in Nambu space.

In order to extract the general behavior of the spin polarization of the superconducting excited state, we employ a perturbation approach. We consider the BdG Hamiltonian within the first order perturbation,

$$\hat{\mathcal{H}} = \hat{H}_0 + \hat{H}', \quad (8)$$

$$\hat{\mathcal{H}}|\Psi_n\rangle = E_n|\Psi_n\rangle, \quad (9)$$

$$\hat{H}_0|\Psi_n^{(0)}\rangle = \varepsilon_n|\Psi_n^{(0)}\rangle. \quad (10)$$

Here, $\hat{\mathcal{H}}$, \hat{H}_0 , and \hat{H}' correspond to the total, the unperturbed, and the perturbing Hamiltonian, respectively. E_n and $|\Psi_n\rangle$ (ε_n and $|\Psi_n^{(0)}\rangle$) are the eigenvalue and the corresponding eigenstate of the total Hamiltonian $\hat{\mathcal{H}}$ (the unperturbed Hamiltonian \hat{H}_0). We assume for convenience of computation that the \mathbf{g} -vector is parallel to the z -axis ($\mathbf{g}(k) = (0, 0, g_z(k))$) and consider only the spin-triplet pairing ($\psi = 0$). Then, the unperturbed and perturbed terms of the Hamiltonian at a given k are expressed by

$$\begin{aligned} \hat{H}_0 &= -\mu\hat{\sigma}_0 \otimes \hat{\tau}_3 + \begin{pmatrix} \hat{h}(k) & 0 \\ 0 & -\hat{h}^t(-k) \end{pmatrix}, \\ \hat{h}(k) &= \begin{pmatrix} \varepsilon(k) + \Lambda g_z(k) & 0 \\ 0 & \varepsilon(k) - \Lambda g_z(k) \end{pmatrix}, \\ \hat{H}' &= \begin{pmatrix} 0 & \hat{\Delta}(k) \\ \hat{\Delta}^\dagger(k) & 0 \end{pmatrix}, \\ \hat{\Delta}(k) &= \begin{pmatrix} \Delta_{\uparrow,\uparrow}(k) & \Delta_{\uparrow,\downarrow}(k) \\ \Delta_{\downarrow,\uparrow}(k) & \Delta_{\downarrow,\downarrow}(k) \end{pmatrix}. \end{aligned}$$

The gap function components for the various spin-triplet configurations are described by the \mathbf{d} -vector,

$$\begin{aligned} \Delta_{\uparrow,\uparrow}(k) &= -d_x(k) + id_y(k), \\ \Delta_{\uparrow,\downarrow}(k) &= \Delta_{\downarrow,\uparrow}(k) = d_z(k), \\ \Delta_{\downarrow,\downarrow}(k) &= d_x(k) + id_y(k). \end{aligned}$$

For the spin-triplet pairing the \mathbf{d} -vector is expressed through the odd-function $F(k)$ in the reciprocal space as

$$\begin{aligned} \mathbf{d}(k) &= (d_x(k), d_y(k), d_z(k)) \\ &= \hat{\mathbf{n}}|\Delta_0|F(k) \\ &= (\sin\theta_d \cos\phi_d, \sin\theta_d \sin\phi_d, \cos\theta_d)|\Delta_0|F(k), \quad (11) \end{aligned}$$

and the gap amplitude $|\Delta_0|$ sets the pairing strength. The eigenstate $|\Psi_1^{(0)}\rangle$ ($|\Psi_3^{(0)}\rangle$) corresponds to $|e, \uparrow\rangle$ ($|h, \uparrow$

\rangle), and $|\Psi_2^{(0)}\rangle$ ($|\Psi_4^{(0)}\rangle$) is related to $|e, \downarrow\rangle$ ($|h, \downarrow\rangle$), respectively. The eigenvalues and the corresponding eigenstates of the unperturbed Hamiltonian \hat{H}_0 are given by

$$\begin{aligned} \varepsilon_1(k) &= -\varepsilon_4(k) = \varepsilon(k) + \Lambda g_z(k), \\ \varepsilon_2(k) &= -\varepsilon_3(k) = \varepsilon(k) - \Lambda g_z(k), \\ |\Psi_1^{(0)}\rangle &= \begin{pmatrix} \hat{\alpha}_+ \\ \hat{0} \end{pmatrix}, \quad |\Psi_2^{(0)}\rangle = \begin{pmatrix} \hat{\alpha}_- \\ \hat{0} \end{pmatrix}, \\ |\Psi_3^{(0)}\rangle &= \begin{pmatrix} \hat{0} \\ \hat{\beta}_+ \end{pmatrix}, \quad |\Psi_4^{(0)}\rangle = \begin{pmatrix} \hat{0} \\ \hat{\beta}_- \end{pmatrix}. \end{aligned}$$

Here, $\hat{\alpha}_\pm$ and $\hat{\beta}_\pm$ denote the eigenstates of $\hat{h}(k)$ and $-\hat{h}^t(-k)$,

$$\hat{\alpha}_+ = \hat{\beta}_+ = \begin{pmatrix} 1 \\ 0 \end{pmatrix}, \quad \hat{\alpha}_- = \hat{\beta}_- = \begin{pmatrix} 0 \\ 1 \end{pmatrix}.$$

For the electron-like band, the perturbation within the first order is zero. It means that the spin polarization for the electron-like band is not modified within the first order perturbation in $|\Delta_0|$. On the other hand, since the eigenvalues and the corresponding eigenstates for the hole-like band change within the first order correction, the spin orientation of the excited state for the hole-like band acquires a non-trivial pattern. Thus, we focus on the hole-like branch of the excited state to investigate the spin texture and we extract the electron component of the spin-polarization for the first excited state of the spectrum. Then, since the spin-singlet component is not affecting the spin-polarization one can set $\psi = 0$ for convenience and clarity of the results presentation. The eigenstates within the first order perturbation $|\Psi_{n=3,4}^{(1)}\rangle$ ($|\Psi_n\rangle = |\Psi_n^{(0)}\rangle + |\Psi_n^{(1)}\rangle + \dots$) are given by

$$\begin{aligned} |\Psi_3^{(1)}\rangle &= -\frac{\hat{\alpha}_+^\dagger \hat{\Delta} \hat{\beta}_+}{2[-\mu + \varepsilon(k)]} \begin{pmatrix} \hat{\alpha}_+ \\ 0 \end{pmatrix} \\ &\quad - \frac{\hat{\alpha}_-^\dagger \hat{\Delta} \hat{\beta}_+}{2[-\mu + \varepsilon(k) - \Lambda g_z(k)]} \begin{pmatrix} \hat{\alpha}_- \\ 0 \end{pmatrix} \\ &= -\frac{\Delta_{\uparrow,\uparrow}}{2[-\mu + \varepsilon(k)]} \begin{pmatrix} \hat{\alpha}_+ \\ 0 \end{pmatrix} \\ &\quad - \frac{\Delta_{\downarrow,\uparrow}}{2[-\mu + \varepsilon(k) - \Lambda g_z(k)]} \begin{pmatrix} \hat{\alpha}_- \\ 0 \end{pmatrix}, \\ |\Psi_4^{(1)}\rangle &= -\frac{\hat{\alpha}_+^\dagger \hat{\Delta} \hat{\beta}_-}{2[-\mu + \varepsilon(k) + \Lambda g_z(k)]} \begin{pmatrix} \hat{\alpha}_+ \\ 0 \end{pmatrix} \\ &\quad - \frac{\hat{\alpha}_-^\dagger \hat{\Delta} \hat{\beta}_-}{2[-\mu + \varepsilon(k)]} \begin{pmatrix} \hat{\alpha}_- \\ 0 \end{pmatrix} \\ &= -\frac{\Delta_{\uparrow,\downarrow}}{2[-\mu + \varepsilon(k) + \Lambda g_z(k)]} \begin{pmatrix} \hat{\alpha}_+ \\ 0 \end{pmatrix} \\ &\quad - \frac{\Delta_{\downarrow,\downarrow}}{2[-\mu + \varepsilon(k)]} \begin{pmatrix} \hat{\alpha}_- \\ 0 \end{pmatrix}. \end{aligned}$$

Then, we can calculate the expectation values of the spin operators for the hole-branch of the first excited state of

the BdG spectrum within the first order perturbation. For $|\langle\Psi_3\rangle$ and $|\langle\Psi_4\rangle$ we have

$$\begin{aligned} & \langle\Psi_3|\tilde{S}_i^e|\Psi_3\rangle \\ &= \frac{|\Delta_{\uparrow,\uparrow}|^2}{4[-\mu+\varepsilon(k)]^2}\hat{\alpha}_+^\dagger\hat{S}_i\hat{\alpha}_+ \\ &+ \frac{|\Delta_{\downarrow,\uparrow}|^2}{4[-\mu+\varepsilon(k)-\Lambda g_z(k)]^2}\hat{\alpha}_-^\dagger\hat{S}_i\hat{\alpha}_- \\ &+ \frac{\Delta_{\uparrow,\uparrow}^*\Delta_{\downarrow,\uparrow}}{4[-\mu+\varepsilon(k)][-\mu+\varepsilon(k)-\Lambda g_z(k)]}\hat{\alpha}_+^\dagger\hat{S}_i\hat{\alpha}_- \\ &+ \frac{\Delta_{\uparrow,\uparrow}\Delta_{\downarrow,\uparrow}^*}{4[-\mu+\varepsilon(k)][-\mu+\varepsilon(k)-\Lambda g_z(k)]}\hat{\alpha}_-^\dagger\hat{S}_i\hat{\alpha}_+, \quad (12) \end{aligned}$$

$$\begin{aligned} & \langle\Psi_4|\tilde{S}_i^e|\Psi_4\rangle \\ &= \frac{|\Delta_{\uparrow,\downarrow}|^2}{4[-\mu+\varepsilon(k)+\Lambda g_z(k)]^2}\hat{\alpha}_+^\dagger\hat{S}_i\hat{\alpha}_+ \\ &+ \frac{|\Delta_{\downarrow,\downarrow}|^2}{4[-\mu+\varepsilon(k)]^2}\hat{\alpha}_-^\dagger\hat{S}_i\hat{\alpha}_- \\ &+ \frac{\Delta_{\downarrow,\downarrow}\Delta_{\uparrow,\downarrow}^*}{4[-\mu+\varepsilon(k)][-\mu+\varepsilon(k)+\Lambda g_z(k)]}\hat{\alpha}_+^\dagger\hat{S}_i\hat{\alpha}_- \\ &+ \frac{\Delta_{\downarrow,\downarrow}^*\Delta_{\uparrow,\downarrow}}{4[-\mu+\varepsilon(k)][-\mu+\varepsilon(k)+\Lambda g_z(k)]}\hat{\alpha}_-^\dagger\hat{S}_i\hat{\alpha}_+. \quad (13) \end{aligned}$$

Here, $\hat{\alpha}_+^\dagger\hat{S}_i\hat{\alpha}_+$ and related terms denote the expectation values of the spin operators in the normal state,

$$\begin{aligned} \hat{\alpha}_+^\dagger\hat{S}_x\hat{\alpha}_+ &= 0, \quad \hat{\alpha}_+^\dagger\hat{S}_y\hat{\alpha}_+ = 0, \\ \hat{\alpha}_+^\dagger\hat{S}_z\hat{\alpha}_+ &= \frac{1}{2}, \\ \hat{\alpha}_-^\dagger\hat{S}_x\hat{\alpha}_- &= 0, \quad \hat{\alpha}_-^\dagger\hat{S}_y\hat{\alpha}_- = 0, \\ \hat{\alpha}_-^\dagger\hat{S}_z\hat{\alpha}_- &= -\frac{1}{2}, \end{aligned}$$

and for the terms of the type $\hat{\alpha}_+^\dagger\hat{S}_i\hat{\alpha}_-$ we have

$$\begin{aligned} \hat{\alpha}_+^\dagger\hat{S}_x\hat{\alpha}_- &= \frac{1}{2}, \quad \hat{\alpha}_+^\dagger\hat{S}_y\hat{\alpha}_- = -\frac{i}{2}, \\ \hat{\alpha}_+^\dagger\hat{S}_z\hat{\alpha}_- &= 0, \quad \hat{\alpha}_-^\dagger\hat{S}_x\hat{\alpha}_+ = \frac{1}{2}, \\ \hat{\alpha}_-^\dagger\hat{S}_y\hat{\alpha}_+ &= \frac{i}{2}, \quad \hat{\alpha}_-^\dagger\hat{S}_z\hat{\alpha}_+ = 0. \end{aligned}$$

Moreover, the \mathbf{d} -vector given in Eq. (11) can be expressed in terms of the relative angle with respect to the \mathbf{g} -vector providing the following quantities,

$$\begin{aligned} |\Delta_{\uparrow,\uparrow}|^2 &= |\Delta_{\downarrow,\downarrow}|^2 = |\Delta_0|^2[F(k)]^2 \sin^2 \theta_d, \\ |\Delta_{\uparrow,\downarrow}|^2 &= |\Delta_{\downarrow,\uparrow}|^2 = |\Delta_0|^2[F(k)]^2 \cos^2 \theta_d, \\ \Delta_{\uparrow,\uparrow}^*\Delta_{\downarrow,\uparrow} &= -|\Delta_0|^2[F(k)]^2 e^{i\phi_d} \sin \theta_d \cos \theta_d, \\ \Delta_{\downarrow,\downarrow}^*\Delta_{\uparrow,\downarrow} &= |\Delta_0|^2[F(k)]^2 e^{-i\phi_d} \sin \theta_d \cos \theta_d. \end{aligned}$$

Hence, the expectation values of the spin operators projected onto the electron space for the hole-like branch of

the first excited state are given by

$$\begin{aligned} & \langle\Psi_3|\tilde{S}_x^e|\Psi_3\rangle \\ &= -\frac{|\Delta_0|^2[F(k)]^2}{2} \frac{\cos \phi_d \sin \theta_d \cos \theta_d}{2[-\mu+\varepsilon(k)][-\mu+\varepsilon(k)-\Lambda g_z(k)]}, \quad (14) \end{aligned}$$

$$\begin{aligned} & \langle\Psi_3|\tilde{S}_y^e|\Psi_3\rangle \\ &= -\frac{|\Delta_0|^2[F(k)]^2}{2} \frac{\sin \phi_d \sin \theta_d \cos \theta_d}{2[-\mu+\varepsilon(k)][-\mu+\varepsilon(k)-\Lambda g_z(k)]}, \quad (15) \end{aligned}$$

$$\begin{aligned} & \langle\Psi_3|\tilde{S}_z^e|\Psi_3\rangle \\ &= \frac{|\Delta_0|^2[F(k)]^2}{2} \\ &\times \left[\frac{\sin^2 \theta_d}{4[-\mu+\varepsilon(k)]^2} - \frac{\cos^2 \theta_d}{4[-\mu+\varepsilon(k)-\Lambda g_z(k)]^2} \right], \quad (16) \end{aligned}$$

$$\begin{aligned} & \langle\Psi_4|\tilde{S}_x^e|\Psi_4\rangle \\ &= \frac{|\Delta_0|^2[F(k)]^2}{2} \frac{\cos \phi_d \sin \theta_d \cos \theta_d}{2[-\mu+\varepsilon(k)][-\mu+\varepsilon(k)+\Lambda g_z(k)]}, \quad (17) \end{aligned}$$

$$\begin{aligned} & \langle\Psi_4|\tilde{S}_y^e|\Psi_4\rangle \\ &= \frac{|\Delta_0|^2[F(k)]^2}{2} \frac{\sin \phi_d \sin \theta_d \cos \theta_d}{2[-\mu+\varepsilon(k)][-\mu+\varepsilon(k)+\Lambda g_z(k)]}, \quad (18) \end{aligned}$$

$$\begin{aligned} & \langle\Psi_4|\tilde{S}_z^e|\Psi_4\rangle \\ &= -\frac{|\Delta_0|^2[F(k)]^2}{2} \\ &\times \left[\frac{\sin^2 \theta_d}{4[-\mu+\varepsilon(k)]^2} - \frac{\cos^2 \theta_d}{4[-\mu+\varepsilon(k)+\Lambda g_z(k)]^2} \right]. \quad (19) \end{aligned}$$

If $|\mu+\varepsilon(k)| \gg |\Lambda g_z(k)|$, we can approximate the above reported expectation values as

$$\langle\Psi_3|\tilde{S}_x^e|\Psi_3\rangle \sim -\frac{|\Delta_0|^2[F(k)]^2}{8} \frac{\cos \phi_d \sin 2\theta_d}{[-\mu+\varepsilon(k)]^2}, \quad (20)$$

$$\langle\Psi_3|\tilde{S}_y^e|\Psi_3\rangle \sim -\frac{|\Delta_0|^2[F(k)]^2}{8} \frac{\sin \phi_d \sin 2\theta_d}{[-\mu+\varepsilon(k)]^2}, \quad (21)$$

$$\langle\Psi_3|\tilde{S}_z^e|\Psi_3\rangle \sim -\frac{|\Delta_0|^2[F(k)]^2}{8} \frac{\cos 2\theta_d}{[-\mu+\varepsilon(k)]^2}, \quad (22)$$

$$\langle\Psi_4|\tilde{S}_x^e|\Psi_4\rangle \sim \frac{|\Delta_0|^2[F(k)]^2}{8} \frac{\cos \phi_d \sin 2\theta_d}{[-\mu+\varepsilon(k)]^2}, \quad (23)$$

$$\langle\Psi_4|\tilde{S}_y^e|\Psi_4\rangle \sim \frac{|\Delta_0|^2[F(k)]^2}{8} \frac{\sin \phi_d \sin 2\theta_d}{[-\mu+\varepsilon(k)]^2}, \quad (24)$$

$$\langle\Psi_4|\tilde{S}_z^e|\Psi_4\rangle \sim \frac{|\Delta_0|^2[F(k)]^2}{8} \frac{\cos 2\theta_d}{[-\mu+\varepsilon(k)]^2}. \quad (25)$$

At this stage, one can evaluate the character of the spin texture from these expectation values of the spin operators. As pointed out in the main text, the relative direction of \mathbf{d} -vector and \mathbf{g} -vector is described by ϕ_d and θ_d ,

and the electron component of the spin polarization for the hole-like branch of the excited state depends on ϕ_d and $2\theta_d$. This result indicates that the spin texture for the hole-like branch of the excited state lies in the plane marked by the \mathbf{d} - and \mathbf{g} -vectors and its direction is determined by the relative angle θ_d between \mathbf{d} -vector and \mathbf{g} -vector. By a suitable rotation of the spin-coordinate, we can deduce the spin texture where \mathbf{d} -vector and \mathbf{g} -vector lies on xy -plane.

On the Fermi surface, $|e, \uparrow\rangle$ and $|h, \downarrow\rangle$ ($|e, \downarrow\rangle$ and $|h, \uparrow\rangle$) are two-fold degenerate. We solve the BdG Hamiltonian on the Fermi surface in the basis ($|e \uparrow\rangle, |e \downarrow\rangle, |h \uparrow\rangle, |h \downarrow\rangle$),

$$\hat{H}(k_F) = \begin{pmatrix} 0 & 0 & \Delta_{\uparrow,\uparrow} & \Delta_{\uparrow,\downarrow} \\ 0 & \varepsilon_2(k_F) & \Delta_{\downarrow,\uparrow} & \Delta_{\downarrow,\downarrow} \\ \Delta_{\uparrow,\uparrow}^* & \Delta_{\downarrow,\uparrow}^* & -\varepsilon_2(k_F) & 0 \\ \Delta_{\uparrow,\downarrow}^* & \Delta_{\downarrow,\downarrow}^* & 0 & 0 \end{pmatrix}, \quad (26)$$

where k_F is the Fermi wave vector. We pick up the basis ($|e \uparrow\rangle, |h \downarrow\rangle$) in this Hamiltonian and obtain the Hamiltonian projected onto the basis ($|e \uparrow\rangle, |h \downarrow\rangle$) near the Fermi level,

$$\tilde{H}(k_F) = \begin{pmatrix} 0 & \Delta_{\uparrow,\downarrow} \\ \Delta_{\uparrow,\downarrow}^* & 0 \end{pmatrix}, \quad (27)$$

with $\Delta_{\uparrow,\downarrow} = |\Delta_0| \cos \theta_d$. Then the eigenvalues are given by

$$E_{\pm} = \pm |\Delta_0| \cos \theta_d, \quad (28)$$

and the corresponding eigenstates in the basis ($|e \uparrow\rangle, |e \downarrow\rangle, |h \uparrow\rangle, |h \downarrow\rangle$) are given by

$$|+\rangle = |-\rangle = \frac{1}{\sqrt{2}} \begin{pmatrix} \hat{a} \\ \hat{b} \end{pmatrix}, \quad \hat{a} = \begin{pmatrix} 1 \\ 0 \end{pmatrix}, \quad \hat{b} = \begin{pmatrix} 0 \\ 1 \end{pmatrix}.$$

We can obtain the eigenvalues of the electron component of the spin operator at k_F point,

$$\langle + | \tilde{S}_i^e | + \rangle = \frac{1}{2} \hat{a}_+^\dagger \hat{S}_i \hat{a}_+,$$

that is,

$$\begin{aligned} \langle + | \tilde{S}_x^e | + \rangle &= \langle + | \tilde{S}_y^e | + \rangle = 0, \\ \langle + | \tilde{S}_z^e | + \rangle &= \frac{1}{2} \hat{a}_+^\dagger \hat{S}_z \hat{a}_+ = \frac{1}{4}. \end{aligned}$$

Thus, the spin texture on the Fermi surface has the same direction as that in the normal state.

In the single orbital model with Rashba-type spin-orbit coupling $\mathbf{g}(\mathbf{k}) = (\sin k_y, -\sin k_x, 0)$, the spin texture in the normal state rotates on the Fermi surface and it is determined by the \mathbf{g} -vector. In the superconducting state, we obtain the spin texture projected onto the electron space at the first excited state and it winds around the point node with the winding number W_S . We call this behavior topological spin winding texture. This topological spin winding texture does not always appear even if

there are point nodes in the bulk. Indeed, if the \mathbf{d} -vector is parallel to the \mathbf{g} -vector on the Fermi surface like for a superconducting state with $d_{x^2-y^2} + f$ -wave pairing symmetry, that is, $\theta_d = 0, \pi$, then, the spin texture for the hole-like branch of the excited state has the same direction as that in the normal state. It means that the spin texture projected onto the electron space does not wind around the point node and the topological spin texture does not appear for this pairing configuration. Therefore, as a general remark, the presence of point nodes does not guarantee the occurrence of a topological spin texture that instead requires a θ_d amplitude that deviates from 0 to π .

A. Spin polarization in the presence of spin-singlet pairing

In the previous section, we have considered only spin-triplet pairing. Here, we discuss the effects of introducing a small amplitude of the spin-singlet pairing to study the case where spin-singlet and spin-triplet pairing coexist. We consider the following gap function,

$$\hat{\Delta} = r_s \hat{\Delta}_S + (1 - r_s) \hat{\Delta}_T.$$

Here, r_s denotes the relative ratio between spin-singlet and spin-triplet pairing amplitudes, and the gap function $\hat{\Delta}_S$ ($\hat{\Delta}_T$) corresponds to the spin-singlet (spin-triplet) pairing. One can easily verify that the spin texture projected onto the electron space in the superconducting state also winds around the point node if the spin-singlet pairing exists.

B. Spin-winding for the B_2 representation in the point group C_{4v}

We have demonstrated the spin-winding for the B_1 representation in the point group C_{4v} in the main text. In this subsection, we mention the spin-winding for the B_2 representation with nodal points on the k_x and k_y -axis. The \mathbf{d} -vector for the B_2 representation is given by

$$d(\mathbf{k}) = (\sin k_x, -\sin k_y, 0).$$

Since this \mathbf{d} -vector is obtained by the $\pi/4$ -rotation of the B_1 representation \mathbf{d} -vector at each k point, we obtain the same spin-winding along the k_x and k_y -axis for the B_2 representation.

II. DERIVATION OF SINGLE ORBITAL EFFECTIVE DESCRIPTION FROM THE THREE-ORBITAL MODEL WITH ATOMIC SPIN-ORBIT AND ORBITAL RASHBA COUPLINGS

In this section, we construct the effective single orbital low-energy description near the Γ point starting from the

three-orbital model which describes a two-dimensional non-centrosymmetric electronic system with tetragonal symmetry including the atomic spin-orbit and the orbital Rashba coupling. The aim is to compare the spin polarization obtained in the single orbital model with that of the full multi-orbital model. The Hamiltonian in the basis $[|\uparrow, \downarrow\rangle \otimes (d_{yz}, d_{zx}, d_{xy})]$ for the normal state¹ is given by

$$\begin{aligned} \hat{H}(\mathbf{k}) &= -\mu\hat{\sigma}_0 \otimes \hat{L}_0 + \hat{\sigma}_0 \otimes \hat{\varepsilon}(\mathbf{k}) \\ &+ \lambda_{\text{SO}} \sum_{i=x,y,z} \hat{\sigma}_i \otimes \hat{L}_i \\ &+ \Delta_{\text{is}}\hat{\sigma}_0 \otimes [g_x(\mathbf{k})\hat{L}_x + g_y(\mathbf{k})\hat{L}_y], \end{aligned} \quad (29)$$

with $g_x(\mathbf{k}) = \sin k_y$, and $g_y(\mathbf{k}) = -\sin k_x$. Here, $\hat{\varepsilon}(\mathbf{k})$ denotes the matrix for the kinetic energy,

$$\hat{\varepsilon}(\mathbf{k}) = \begin{pmatrix} \varepsilon_{yz}(\mathbf{k}) & 0 & 0 \\ 0 & \varepsilon_{zx}(\mathbf{k}) & 0 \\ 0 & 0 & \varepsilon_{xy}(\mathbf{k}) \end{pmatrix},$$

and the kinetic energy for each orbital is given by

$$\begin{aligned} \varepsilon_{yz}(\mathbf{k}) &= 2t_1(1 - \cos k_y) + 2t_3(1 - \cos k_x), \\ \varepsilon_{zx}(\mathbf{k}) &= 2t_1(1 - \cos k_x) + 2t_3(1 - \cos k_y), \\ \varepsilon_{xy}(\mathbf{k}) &= 4t_2 - 2t_2(\cos k_x + \cos k_y) + \Delta_t, \end{aligned}$$

where $t_1 = t = 0.10$, $t_2 = t$, and $t_3 = 0.10t$ are the hopping integral with representative amplitudes, Δ_t is the crystal field potential associated with the breaking of the cubic symmetry. λ_{SO} and Δ_{is} are the spin-orbit coupling constant and the inversion symmetry breaking terms, respectively. \hat{L}_i ($i = x, y, z$) in the basis (d_{yz}, d_{zx}, d_{xy}) denotes the orbital angular momentum operator which is projection of the $L = 2$ angular momentum operator onto the t_{2g} subspace,

$$\hat{L}_x = \begin{pmatrix} 0 & 0 & 0 \\ 0 & 0 & i \\ 0 & -i & 0 \end{pmatrix}, \hat{L}_y = \begin{pmatrix} 0 & 0 & -i \\ 0 & 0 & 0 \\ i & 0 & 0 \end{pmatrix}, \hat{L}_z = \begin{pmatrix} 0 & i & 0 \\ -i & 0 & 0 \\ 0 & 0 & 0 \end{pmatrix},$$

and \hat{L}_0 is a 3×3 identity matrix. In this system, there are six nondegenerated bands at $\lambda_{\text{SO}} \neq 0$ and $\Delta_{\text{is}} \neq 0$. We define the index n of the bands labelling the configurations from the lowest energy (i.e. $n = 1$) to the highest one (i.e. $n = 6$).

In the superconducting state, the BdG Hamiltonian in the three-orbital model is given by

$$\hat{H}_{\text{BdG}} = \begin{pmatrix} \hat{H}(\mathbf{k}) & \hat{\Delta} \\ \hat{\Delta}^\dagger & -\hat{H}^t(-\mathbf{k}) \end{pmatrix}. \quad (30)$$

Here, the superconducting order parameter associated with orbitals α and β can be classified as an isotropic (s -wave) spin-triplet/orbital-singlet $\mathbf{d}^{(\alpha,\beta)}$ -vector and s -wave spin-singlet/orbital-triplet with amplitude $\psi^{(\alpha,\beta)}$ or

as a mixing of both configurations. With these assumptions, one can generally describe the isotropic order parameter with spin-singlet and triplet components as

$$\begin{aligned} \hat{\Delta}_{\alpha,\beta} &= \begin{pmatrix} \hat{\Delta}_{\alpha\uparrow,\beta\uparrow} & \hat{\Delta}_{\alpha\uparrow,\beta\downarrow} \\ \hat{\Delta}_{\alpha\downarrow,\beta\uparrow} & \hat{\Delta}_{\alpha\downarrow,\beta\downarrow} \end{pmatrix}, \\ &= i\hat{\sigma}_y [\psi^{(\alpha,\beta)} + \hat{\boldsymbol{\sigma}} \cdot \mathbf{d}^{(\alpha,\beta)}], \end{aligned}$$

with α and β standing for the orbital index, and having for each channel three possible orbital flavors. Furthermore, owing to the selected tetragonal crystal symmetry, one can achieve three different types of inter-orbital pairings. The spin-singlet configurations are orbital triplets and can be described by a symmetric superposition of opposite spin states in different orbitals. On the other hand, spin-triplet components can be expressed by means of the following \mathbf{d} -vectors:

$$\begin{aligned} \mathbf{d}^{(xy,yz)} &= (d_x^{(xy,yz)}, d_y^{(xy,yz)}, d_z^{(xy,yz)}), \\ \mathbf{d}^{(xy,zx)} &= (d_x^{(xy,zx)}, d_y^{(xy,zx)}, d_z^{(xy,zx)}), \\ \mathbf{d}^{(yz,zx)} &= (d_x^{(yz,zx)}, d_y^{(yz,zx)}, d_z^{(yz,zx)}). \end{aligned}$$

In the Supplemental Material, we consider the inter-orbital local pairings for the A_1 and B_1 representations in the point group C_{4v} ².

To obtain the effective single orbital model for the normal state electronic structure near the Γ -point from the three-orbital model we employ the following perturbation scheme separating the Hamiltonian in two parts,

$$\hat{H} = \hat{H}_0 + \hat{H}', \quad (31)$$

$$\hat{H}_0 = \hat{\varepsilon}(\mathbf{k}), \quad (32)$$

$$\hat{H}' = \lambda_{\text{SO}} \sum_{i=x,y,z} \hat{\sigma}_i \otimes \hat{L}_i \quad (33)$$

$$+ \Delta_{\text{is}}\hat{\sigma}_0 \otimes [g_x(\mathbf{k})\hat{L}_x + g_y(\mathbf{k})\hat{L}_y]. \quad (34)$$

Importantly, due to the two-dimensional confinement, the d_{xy} -orbital is generally well separated from the (d_{zx}, d_{yz}) -orbitals by the crystal field potential Δ_t . In the normal state of \hat{H}_0 , the d_{xy} -orbital has the lowest energy among the three orbitals and the energy of the d_{xy} -orbital is $-\Delta_t$ lower than d_{yz} and d_{zx} -orbitals. We can consider the following process $|xy, \uparrow\rangle \rightarrow |xy, \downarrow\rangle$ within the second order perturbation,

$$\begin{aligned} -\frac{\langle xy, \downarrow | \hat{H}' | yz, \uparrow \rangle \langle yz, \uparrow | \hat{H}' | xy, \uparrow \rangle}{E_{yz} - E_{xy}} &= \frac{i\lambda_{\text{SO}}\Delta_{\text{is}} \sin k_x}{\Delta_t}, \\ -\frac{\langle xy, \downarrow | \hat{H}' | yz, \downarrow \rangle \langle yz, \downarrow | \hat{H}' | xy, \uparrow \rangle}{E_{yz} - E_{xy}} &= \frac{i\lambda_{\text{SO}}\Delta_{\text{is}} \sin k_x}{\Delta_t}, \\ -\frac{\langle xy, \downarrow | \hat{H}' | zx, \uparrow \rangle \langle zx, \uparrow | \hat{H}' | xy, \uparrow \rangle}{E_{zx} - E_{xy}} &= -\frac{\lambda_{\text{SO}}\Delta_{\text{is}} \sin k_y}{\Delta_t}, \\ -\frac{\langle xy, \downarrow | \hat{H}' | zx, \downarrow \rangle \langle zx, \downarrow | \hat{H}' | xy, \uparrow \rangle}{E_{zx} - E_{xy}} &= -\frac{\lambda_{\text{SO}}\Delta_{\text{is}} \sin k_y}{\Delta_t}, \end{aligned}$$

with $E_{yz} = -\Delta_t$ and $E_{yz} = 0$. Likewise, we can consider the following process $|xy, \downarrow\rangle \rightarrow |xy, \uparrow\rangle$ within the second order perturbation,

$$\begin{aligned} -\frac{\langle xy, \uparrow | \hat{H}' | yz, \downarrow \rangle \langle yz, \downarrow | \hat{H}' | xy, \downarrow \rangle}{E_{yz} - E_{xy}} &= -\frac{i\lambda_{\text{SO}}\Delta_{\text{is}} \sin k_x}{\Delta_t}, \\ -\frac{\langle xy, \uparrow | \hat{H}' | yz, \uparrow \rangle \langle yz, \uparrow | \hat{H}' | xy, \downarrow \rangle}{E_{yz} - E_{xy}} &= -\frac{i\lambda_{\text{SO}}\Delta_{\text{is}} \sin k_x}{\Delta_t}, \\ -\frac{\langle xy, \uparrow | \hat{H}' | zx, \downarrow \rangle \langle zx, \downarrow | \hat{H}' | xy, \downarrow \rangle}{E_{zx} - E_{xy}} &= -\frac{\lambda_{\text{SO}}\Delta_{\text{is}} \sin k_y}{\Delta_t}, \\ -\frac{\langle xy, \uparrow | \hat{H}' | zx, \uparrow \rangle \langle zx, \uparrow | \hat{H}' | xy, \downarrow \rangle}{E_{zx} - E_{xy}} &= -\frac{\lambda_{\text{SO}}\Delta_{\text{is}} \sin k_y}{\Delta_t}, \end{aligned}$$

then, in the subspace spanned by the states $|xy, \downarrow\rangle, |xy, \uparrow\rangle$ we obtain the effective low energy Hamiltonian in the normal state,

$$\begin{aligned} \tilde{h}(\mathbf{k}) &= \begin{pmatrix} \varepsilon_{\uparrow, \uparrow}(\mathbf{k}) & \varepsilon_{\uparrow, \downarrow}(\mathbf{k}) \\ \varepsilon_{\downarrow, \uparrow}(\mathbf{k}) & \varepsilon_{\downarrow, \downarrow}(\mathbf{k}) \end{pmatrix}, \\ &= \varepsilon_{xy}(\mathbf{k})\hat{\sigma}_0 + \Lambda_{\text{R}}[g_x(\mathbf{k})\hat{\sigma}_x + g_y(\mathbf{k})\hat{\sigma}_y], \\ \mathbf{g}(\mathbf{k}) &= (\sin k_y, -\sin k_x, 0), \end{aligned}$$

with $\Lambda_{\text{R}} = -2\lambda_{\text{SO}}\Delta_{\text{is}}/\Delta_t$. Then, the elements of the Hamiltonian in the effective model $\varepsilon_{\downarrow, \uparrow}(\mathbf{k})$ and $\varepsilon_{\uparrow, \downarrow}(\mathbf{k})$ are derived as

$$\begin{aligned} \varepsilon_{\downarrow, \uparrow}(\mathbf{k}) &= -\sum_{l \neq xy, \sigma} \frac{\langle xy, \downarrow | \hat{H}' | l, \sigma \rangle \langle l, \sigma | \hat{H}' | xy, \uparrow \rangle}{E_l - E_{xy}} \\ &= \Lambda_{\text{R}}[\sin k_y - i \sin k_x], \\ \varepsilon_{\uparrow, \downarrow}(\mathbf{k}) &= -\sum_{l \neq xy, \sigma} \frac{\langle xy, \uparrow | \hat{H}' | l, \sigma \rangle \langle l, \sigma | \hat{H}' | xy, \downarrow \rangle}{E_l - E_{xy}} \\ &= \Lambda_{\text{R}}[\sin k_y + i \sin k_x], \end{aligned}$$

where $l = yz, zx, xy$ is the index of the d -orbital and $\sigma = \uparrow, \downarrow$ indicate the spin polarizations. On the other hand, because there are no processes $|xy, \uparrow\rangle \rightarrow |xy, \uparrow\rangle$ and $|xy, \downarrow\rangle \rightarrow |xy, \downarrow\rangle$ within the second order perturbation, we obtain

$$\varepsilon_{\uparrow, \uparrow}(\mathbf{k}) = \varepsilon_{\downarrow, \downarrow}(\mathbf{k}) = \varepsilon_{xy}(\mathbf{k}). \quad (35)$$

The effective low energy description is then expressed by a single-orbital model with a Rashba-type spin-orbit coupling.

In a similar fashion, for the superconducting state one

consider the following perturbation scheme,

$$\begin{aligned} \hat{H}_{\text{BdG}} &= \hat{H}_{\text{BdG}}^0 + \hat{H}'_{\text{BdG}}, \\ \hat{H}_{\text{BdG}}^0 &= \begin{pmatrix} \hat{\varepsilon}(\mathbf{k}) & 0 \\ 0 & -\hat{\varepsilon}(-\mathbf{k}) \end{pmatrix}, \\ \hat{H}'_{\text{BdG}} &= \begin{pmatrix} \hat{H}_{\text{SO}} & 0 \\ 0 & -\hat{H}_{\text{SO}} \end{pmatrix} + \begin{pmatrix} \hat{H}_{\text{is}}(\mathbf{k}) & 0 \\ 0 & -\hat{H}_{\text{is}}^t(-\mathbf{k}) \end{pmatrix} \\ &\quad + \begin{pmatrix} 0 & \hat{\Delta} \\ \hat{\Delta}^\dagger & 0 \end{pmatrix}, \\ \hat{H}_{\text{SO}} &= \lambda_{\text{SO}} \sum_{i=x,y,z} \hat{\sigma}_i \otimes \hat{L}_i, \\ \hat{H}_{\text{is}}(\mathbf{k}) &= \Delta_{\text{is}}\hat{\sigma}_0 \otimes [g_x(\mathbf{k})\hat{L}_x + g_y(\mathbf{k})\hat{L}_y]. \end{aligned}$$

The energy of $|yz, \sigma, h\rangle$ and $|zx, \sigma, h\rangle$ states is $-\Delta_t$ lower than that of $|xy, \sigma, h\rangle$ state. Here $\sigma = \uparrow, \downarrow$ denotes the spin of the electron and hole. The effective BdG Hamiltonian from the three-orbital model is given by

$$\begin{aligned} \tilde{H}_{\text{BdG}} &= \begin{pmatrix} \tilde{h}(\mathbf{k}) & \tilde{\Delta} \\ \tilde{\Delta}^\dagger & -\tilde{h}^t(-\mathbf{k}) \end{pmatrix}, \\ \tilde{\Delta}(\mathbf{k}) &= \begin{pmatrix} \Delta_{\uparrow, \uparrow} & \Delta_{\uparrow, \downarrow} \\ \Delta_{\downarrow, \uparrow} & \Delta_{\downarrow, \downarrow} \end{pmatrix}, \\ &= \begin{pmatrix} \Delta_{\uparrow, \uparrow} & \Delta_{\uparrow, \downarrow}^{\text{S}} + \Delta_{\uparrow, \downarrow}^{\text{T}} \\ \Delta_{\downarrow, \uparrow}^{\text{S}} + \Delta_{\downarrow, \uparrow}^{\text{T}} & \Delta_{\downarrow, \downarrow} \end{pmatrix}. \end{aligned}$$

This effective Hamiltonian can be obtained by the following processes within the second order perturbation,

$$\begin{aligned} &-\frac{\langle xy, \uparrow, e | \hat{H}'_{\text{BdG}} | yz, \uparrow, h \rangle \langle yz, \uparrow, h | \hat{H}'_{\text{BdG}} | xy, \uparrow, h \rangle}{E_{yz, h} - E_{xy}} \\ &= \frac{i\Delta_{\text{is}}\Delta_{xy\uparrow, yz\uparrow} \sin k_x}{\Delta_t}, \\ &-\frac{\langle xy, \uparrow, e | \hat{H}'_{\text{BdG}} | yz, \uparrow, e \rangle \langle yz, \uparrow, e | \hat{H}'_{\text{BdG}} | xy, \uparrow, h \rangle}{E_{yz, e} - E_{xy}} \\ &= \frac{i\Delta_{\text{is}}\Delta_{xy\uparrow, yz\uparrow} \sin k_x}{\Delta_t}, \\ &-\frac{\langle xy, \uparrow, e | \hat{H}'_{\text{BdG}} | zx, \uparrow, h \rangle \langle zx, \uparrow, h | \hat{H}'_{\text{BdG}} | xy, \uparrow, h \rangle}{E_{yz, h} - E_{xy}} \\ &= \frac{i\Delta_{\text{is}}\Delta_{xy\uparrow, zx\uparrow} \sin k_y}{\Delta_t}, \\ &-\frac{\langle xy, \uparrow, e | \hat{H}'_{\text{BdG}} | zx, \uparrow, e \rangle \langle zx, \uparrow, e | \hat{H}'_{\text{BdG}} | xy, \uparrow, h \rangle}{E_{yz, e} - E_{xy}} \\ &= \frac{i\Delta_{\text{is}}\Delta_{xy\uparrow, zx\uparrow} \sin k_y}{\Delta_t}, \end{aligned}$$

$$\begin{aligned}
& - \frac{\langle xy, \downarrow, e | \hat{H}'_{\text{BdG}} | yz, \downarrow, h \rangle \langle yz, \downarrow, h | \hat{H}'_{\text{BdG}} | xy, \uparrow, h \rangle}{E_{yz,h} - E_{xy}} \\
& = \frac{-\lambda_{\text{SO}} \Delta_{xy\downarrow,yz\downarrow}}{\Delta_t}, \\
& - \frac{\langle xy, \downarrow, e | \hat{H}'_{\text{BdG}} | yz, \downarrow, e \rangle \langle yz, \downarrow, e | \hat{H}'_{\text{BdG}} | xy, \uparrow, h \rangle}{E_{yz,e} - E_{xy}} \\
& = \frac{\lambda_{\text{SO}} \Delta_{xy\uparrow,yz\uparrow}}{-\Delta_t}, \\
& - \frac{\langle xy, \downarrow, e | \hat{H}'_{\text{BdG}} | zx, \downarrow, h \rangle \langle zx, \downarrow, h | \hat{H}'_{\text{BdG}} | xy, \uparrow, h \rangle}{E_{zx,h} - E_{xy}} \\
& = \frac{i\lambda_{\text{SO}} \Delta_{xy\downarrow,zx\downarrow}}{\Delta_t}, \\
& - \frac{\langle xy, \downarrow, e | \hat{H}'_{\text{BdG}} | zx, \downarrow, e \rangle \langle zx, \downarrow, e | \hat{H}'_{\text{BdG}} | xy, \uparrow, h \rangle}{E_{zx,e} - E_{xy}} \\
& = -\frac{i\lambda_{\text{SO}} \Delta_{xy\uparrow,zx\uparrow}}{\Delta_t},
\end{aligned}$$

$$\begin{aligned}
& - \frac{\langle xy, \uparrow, e | \hat{H}'_{\text{BdG}} | yz, \uparrow, h \rangle \langle yz, \uparrow, h | \hat{H}'_{\text{BdG}} | xy, \downarrow, h \rangle}{E_{yz,h} - E_{xy}} \\
& = \frac{\lambda_{\text{SO}} \Delta_{xy\uparrow,yz\uparrow}}{\Delta_t}, \\
& - \frac{\langle xy, \uparrow, e | \hat{H}'_{\text{BdG}} | yz, \downarrow, e \rangle \langle yz, \downarrow, e | \hat{H}'_{\text{BdG}} | xy, \downarrow, h \rangle}{E_{yz,e} - E_{xy}} \\
& = \frac{-\lambda_{\text{SO}} \Delta_{xy\downarrow,yz\downarrow}}{-\Delta_t}, \\
& - \frac{\langle xy, \uparrow, e | \hat{H}'_{\text{BdG}} | zx, \uparrow, h \rangle \langle zx, \uparrow, h | \hat{H}'_{\text{BdG}} | xy, \downarrow, h \rangle}{E_{zx,h} - E_{xy}} \\
& = \frac{i\lambda_{\text{SO}} \Delta_{xy\uparrow,zx\uparrow}}{\Delta_t}, \\
& - \frac{\langle xy, \uparrow, e | \hat{H}'_{\text{BdG}} | zx, \downarrow, e \rangle \langle zx, \downarrow, e | \hat{H}'_{\text{BdG}} | xy, \downarrow, h \rangle}{E_{zx,e} - E_{xy}} \\
& = \frac{i\lambda_{\text{SO}} \Delta_{xy\downarrow,yz\downarrow}}{-\Delta_t},
\end{aligned}$$

$$\begin{aligned}
& - \frac{\langle xy, \downarrow, e | \hat{H}'_{\text{BdG}} | yz, \downarrow, e \rangle \langle yz, \downarrow, e | \hat{H}'_{\text{BdG}} | xy, \uparrow, h \rangle}{E_{yz,e} - E_{xy}} \\
& = \frac{-i\Delta_{\text{is}} \Delta_{xy\uparrow,yz\downarrow} \sin k_x}{\Delta_t}, \\
& - \frac{\langle xy, \downarrow, e | \hat{H}'_{\text{BdG}} | yz, \uparrow, h \rangle \langle yz, \uparrow, h | \hat{H}'_{\text{BdG}} | xy, \uparrow, h \rangle}{E_{yz,h} - E_{xy}} \\
& = \frac{i\Delta_{\text{is}} \Delta_{xy\uparrow,yz\downarrow} \sin k_x}{-\Delta_t}, \\
& - \frac{\langle xy, \downarrow, e | \hat{H}'_{\text{BdG}} | zx, \downarrow, e \rangle \langle zx, \downarrow, e | \hat{H}'_{\text{BdG}} | xy, \uparrow, h \rangle}{E_{zx,e} - E_{xy}} \\
& = \frac{-i\Delta_{\text{is}} \Delta_{xy\uparrow,zx\downarrow} \sin k_y}{\Delta_t}, \\
& - \frac{\langle xy, \downarrow, e | \hat{H}'_{\text{BdG}} | zx, \uparrow, h \rangle \langle zx, \uparrow, h | \hat{H}'_{\text{BdG}} | xy, \uparrow, h \rangle}{E_{zx,h} - E_{xy}} \\
& = -\frac{i\Delta_{\text{is}} \Delta_{xy\uparrow,zx\downarrow} \sin k_y}{\Delta_t},
\end{aligned}$$

$$\begin{aligned}
& - \frac{\langle xy, \uparrow, e | \hat{H}'_{\text{BdG}} | yz, \uparrow, e \rangle \langle yz, \uparrow, e | \hat{H}'_{\text{BdG}} | xy, \downarrow, h \rangle}{E_{yz,e} - E_{xy}} \\
& = -\frac{i\Delta_{\text{is}} \Delta_{xy\downarrow,yz\uparrow} \sin k_x}{\Delta_t}, \\
& - \frac{\langle xy, \uparrow, e | \hat{H}'_{\text{BdG}} | yz, \downarrow, h \rangle \langle yz, \downarrow, h | \hat{H}'_{\text{BdG}} | xy, \downarrow, h \rangle}{E_{yz,h} - E_{xy}} \\
& = -\frac{i\Delta_{\text{is}} \Delta_{xy\downarrow,yz\uparrow} \sin k_x}{\Delta_t}, \\
& - \frac{\langle xy, \uparrow, e | \hat{H}'_{\text{BdG}} | zx, \uparrow, e \rangle \langle zx, \uparrow, e | \hat{H}'_{\text{BdG}} | xy, \downarrow, h \rangle}{E_{zx,e} - E_{xy}} \\
& = -\frac{i\Delta_{\text{is}} \Delta_{xy\downarrow,zx\uparrow} \sin k_x}{\Delta_t}, \\
& - \frac{\langle xy, \uparrow, e | \hat{H}'_{\text{BdG}} | zx, \downarrow, h \rangle \langle zx, \downarrow, h | \hat{H}'_{\text{BdG}} | xy, \downarrow, h \rangle}{E_{zx,h} - E_{xy}} \\
& = -\frac{i\Delta_{\text{is}} \Delta_{xy\downarrow,zx\uparrow} \sin k_x}{\Delta_t},
\end{aligned}$$

$$\begin{aligned}
& - \frac{\langle xy, \downarrow, e | \hat{H}'_{\text{BdG}} | yz, \downarrow, h \rangle \langle yz, \downarrow, h | \hat{H}'_{\text{BdG}} | xy, \downarrow, h \rangle}{E_{yz, h} - E_{xy}} \\
& = \frac{i\Delta_{\text{is}} \Delta_{xy\downarrow, yz\downarrow} \sin k_x}{\Delta_t}, \\
& - \frac{\langle xy, \downarrow, e | \hat{H}'_{\text{BdG}} | yz, \downarrow, e \rangle \langle yz, \downarrow, e | \hat{H}'_{\text{BdG}} | xy, \downarrow, h \rangle}{E_{yz, e} - E_{xy}} \\
& = \frac{i\Delta_{\text{is}} \Delta_{xy\downarrow, yz\downarrow} \sin k_x}{\Delta_t}, \\
& - \frac{\langle xy, \downarrow, e | \hat{H}'_{\text{BdG}} | zx, \downarrow, h \rangle \langle zx, \downarrow, h | \hat{H}'_{\text{BdG}} | xy, \downarrow, h \rangle}{E_{zx, h} - E_{xy}} \\
& = \frac{i\Delta_{\text{is}} \Delta_{xy\downarrow, zx\downarrow} \sin k_x}{\Delta_t}, \\
& - \frac{\langle xy, \downarrow, e | \hat{H}'_{\text{BdG}} | zx, \downarrow, e \rangle \langle zx, \downarrow, e | \hat{H}'_{\text{BdG}} | xy, \downarrow, h \rangle}{E_{zx, e} - E_{xy}} \\
& = \frac{i\Delta_{\text{is}} \Delta_{xy\downarrow, zx\downarrow} \sin k_x}{\Delta_t},
\end{aligned}$$

with $E_{yz, h} = E_{zx, h} = \Delta_t$ and $E_{yz, e} = E_{zx, e} = -\Delta_t$. Then, we obtain the elements of the BdG Hamiltonian in the effective single-orbital description for the d_{xy} -band $\Delta_{\uparrow, \uparrow}$, $\Delta_{\uparrow, \downarrow}$, $\Delta_{\downarrow, \uparrow}$, and $\Delta_{\downarrow, \downarrow}$,

$$\begin{aligned}
\Delta_{\uparrow, \uparrow} & = - \sum_{l \neq xy, \sigma, \tau} \frac{\langle xy, \uparrow, e | \hat{H}'_{\text{BdG}} | l, \sigma, \tau \rangle \langle l, \sigma, \tau | \hat{H}'_{\text{BdG}} | xy, \uparrow, h \rangle}{E_{l, \tau} - E_{xy}} \\
& = \frac{2i\Delta_{\text{is}}}{\Delta_t} [\Delta_{xy\uparrow, yz\uparrow} \sin k_x + \Delta_{xy\uparrow, zx\uparrow} \sin k_y],
\end{aligned}$$

$$\begin{aligned}
\Delta_{\downarrow, \uparrow} & = - \sum_{l \neq xy, \sigma, \tau} \frac{\langle xy, \downarrow, e | \hat{H}'_{\text{BdG}} | l, \sigma, \tau \rangle \langle l, \sigma, \tau | \hat{H}'_{\text{BdG}} | xy, \uparrow, h \rangle}{E_{l, \tau} - E_{xy}} \\
& = \Delta_{\downarrow, \uparrow}^{\text{S}} + \Delta_{\downarrow, \uparrow}^{\text{T}}.
\end{aligned}$$

$$\begin{aligned}
\Delta_{\downarrow, \uparrow}^{\text{S}} & = - \frac{i\lambda_{\text{SO}}}{\Delta_t} [\Delta_{xy\uparrow, yz\uparrow} + \Delta_{xy\downarrow, yz\downarrow} \\
& \quad + i\Delta_{xy\uparrow, zx\uparrow} - i\Delta_{xy\downarrow, zx\downarrow}], \\
\Delta_{\downarrow, \uparrow}^{\text{T}} & = - \frac{2i\Delta_{\text{is}}}{\Delta_t} [\Delta_{xy\uparrow, yz\downarrow} \sin k_x + \Delta_{xy\uparrow, zx\downarrow} \sin k_y].
\end{aligned}$$

$$\begin{aligned}
\Delta_{\uparrow, \downarrow} & = - \sum_{l \neq xy, \sigma, \tau} \frac{\langle xy, \uparrow, e | \hat{H}'_{\text{BdG}} | l, \sigma, \tau \rangle \langle l, \sigma, \tau | \hat{H}'_{\text{BdG}} | xy, \downarrow, h \rangle}{E_{l, \tau} - E_{xy}} \\
& = \Delta_{\uparrow, \downarrow}^{\text{S}} + \Delta_{\uparrow, \downarrow}^{\text{T}},
\end{aligned}$$

$$\begin{aligned}
\Delta_{\uparrow, \downarrow}^{\text{S}} & = \frac{i\lambda_{\text{SO}}}{\Delta_t} [\Delta_{xy\uparrow, yz\uparrow} + \Delta_{xy\downarrow, yz\downarrow} \\
& \quad + i\Delta_{xy\uparrow, zx\uparrow} - i\Delta_{xy\downarrow, zx\downarrow}], \\
\Delta_{\uparrow, \downarrow}^{\text{T}} & = - \frac{2i\Delta_{\text{is}}}{\Delta_t} [\Delta_{xy\downarrow, yz\uparrow} \sin k_x + \Delta_{xy\downarrow, zx\uparrow} \sin k_y],
\end{aligned}$$

$$\begin{aligned}
\Delta_{\downarrow, \downarrow} & = - \sum_{l \neq xy, \sigma, \tau} \frac{\langle xy, \downarrow, e | \hat{H}'_{\text{BdG}} | l, \sigma, \tau \rangle \langle l, \sigma, \tau | \hat{H}'_{\text{BdG}} | xy, \downarrow, h \rangle}{E_{l, \tau} - E_{xy}} \\
& = \frac{2i\Delta_{\text{is}}}{\Delta_t} [\Delta_{xy\downarrow, yz\downarrow} \sin k_x + \Delta_{xy\downarrow, zx\downarrow} \sin k_y],
\end{aligned}$$

where $\tau = e, h$ is the index of electron and hole space and superscript S and T are the spin-singlet and spin-triplet pairing in the (\uparrow, \downarrow) sector of the gap function, respectively.

For the B_1 representation in the point group C_{4v} , the interorbital pairing in the three-orbital model is described by

$$\begin{aligned}
\psi^{(xy, yz)} & = \psi^{(xy, zx)} = \psi^{(yz, zx)} = 0, \\
\mathbf{d}^{(yz, zx)} & = 0, \\
d_z^{(xy, yz)} & = d_z^{(xy, zx)} = d_y^{(xy, zx)} = d_x^{(xy, yz)} = 0, \\
d_x^{(xy, zx)} & = d_y^{(xy, yz)}.
\end{aligned}$$

Then, the gap function in the effective model is

$$\begin{aligned}
\Delta_{\uparrow, \uparrow} & = |\Delta_0^{\text{T}}| (-\sin k_y + i \sin k_x), \\
\Delta_{\uparrow, \downarrow} & = \Delta_{\downarrow, \uparrow} = 0, \\
\Delta_{\downarrow, \downarrow} & = |\Delta_0^{\text{T}}| (\sin k_y + i \sin k_x),
\end{aligned}$$

with $|\Delta_0^{\text{T}}| = |2i\Delta_0|d_y^{(xy, yz)}/\Delta_t$. Hence, we can obtain the \mathbf{d} -vector for the B_1 representation in the effective model:

$$\begin{aligned}
d_x(\mathbf{k}) & = \frac{1}{2} [\Delta_{\downarrow, \downarrow} - \Delta_{\uparrow, \uparrow}] = |\Delta_0^{\text{T}}| \sin k_y, \\
d_y(\mathbf{k}) & = \frac{1}{2i} [\Delta_{\uparrow, \uparrow} + \Delta_{\downarrow, \downarrow}] = |\Delta_0^{\text{T}}| \sin k_x, \\
d_z(\mathbf{k}) & = \Delta_{\uparrow, \downarrow}^{\text{T}} = 0.
\end{aligned}$$

It corresponds to the base functions of the spin-triplet pairing for the B_1 representation in the C_{4v} point group. On the other hand, we obtain the gap function in the effective model for the A_1 representation,

$$\begin{aligned}
\Delta_{\uparrow, \uparrow} & = |\Delta_0^{\text{T}}| (\sin k_y + i \sin k_x), \\
\Delta_{\uparrow, \downarrow}^{\text{T}} & = \Delta_{\downarrow, \uparrow}^{\text{T}} = 0, \\
\Delta_{\uparrow, \downarrow}^{\text{S}} & = -\Delta_{\downarrow, \uparrow}^{\text{S}} = |\Delta_0^{\text{S}}|, \\
\Delta_{\downarrow, \downarrow} & = |\Delta_0^{\text{T}}| (-\sin k_y + i \sin k_x), \\
|\Delta_0^{\text{S}}| & = - \frac{4\lambda_{\text{SO}} d_y^{(xy, yz)}}{\Delta_t},
\end{aligned}$$

from the following interorbital pairing,

$$\begin{aligned}
\psi^{(xy, yz)} & = \psi^{(xy, zx)} = \psi^{(yz, zx)} = 0, \\
d_x^{(yz, zx)} & = d_y^{(yz, zx)} = 0, \\
d_z^{(xy, yz)} & = d_z^{(xy, zx)} = d_y^{(xy, zx)} = d_x^{(xy, yz)} = 0, \\
d_z^{(yz, zx)} & = -d_z^{(zx, yz)}, \\
d_x^{(xy, zx)} & = -d_y^{(xy, yz)}.
\end{aligned}$$

Therefore, the pairings for the A_1 representation in the effective single-orbital model are

$$\begin{aligned}\psi &= \Delta_{\uparrow,\downarrow}^S = |\Delta_0^S|, \\ d_x(\mathbf{k}) &= \frac{1}{2}[\Delta_{\downarrow,\downarrow} - \Delta_{\uparrow,\uparrow}] = -|\Delta_0^T| \sin k_y, \\ d_y(\mathbf{k}) &= \frac{1}{2i}[\Delta_{\uparrow,\uparrow} + \Delta_{\downarrow,\downarrow}] = |\Delta_0^T| \sin k_x, \\ d_z(\mathbf{k}) &= \Delta_{\uparrow,\downarrow}^T = 0.\end{aligned}$$

This \mathbf{d} -vector corresponds to the $s + p$ -wave for the A_1 representation in the C_{4v} point group and it is parallel to \mathbf{g} -vector in the Brillouin zone (BZ).

For the B_1 representation with point nodes in the diagonal direction, the spin texture lies in the xy -plane and the topological spin texture appears around the point node in the effective single orbital model. It means that the topological spin winding texture for the lowest bands 1 and 2 in the three-orbital model can be well described by the single orbital model. On the other hand, for the A_1 representation with the fully gapped state, the spin texture is defined in xy -plane, however, topological spin texture does not appear because \mathbf{d} -vector is parallel to \mathbf{g} -vector in the BZ.

III. SPIN-ORBITAL TEXTURE IN THE THREE-ORBITAL MODEL

In this section, we study the spin-orbital texture in the normal state and the electron projection of the spin polarization in the superconducting state for the three-orbital model in the reciprocal space. Similar to the spin texture, we define the orbital texture by the expectation values of the angular momentum operators.

From the diagonalization of the Hamiltonian in the three-orbital model in the normal state, we obtain the six energy bands and the six corresponding eigenstates. Then, in order to determine the spin-orbital polarizations, we calculate the six expectation values of the orbital angular momentum operator \hat{L}_i and the spin operator \hat{S}_i for the corresponding eigenstates. The spin-orbital polarization can be expressed in a compact notation as

$$\begin{aligned}\langle \hat{A} \rangle_{n,\mathbf{k}} &\equiv \langle \phi_n(\mathbf{k}) | \hat{A} | \phi_n(\mathbf{k}) \rangle, \\ \hat{A} &= \hat{L}_x, \hat{L}_y, \hat{L}_z, \hat{S}_x, \hat{S}_y, \hat{S}_z,\end{aligned}$$

where $|\phi_n(\mathbf{k})\rangle$ ($n = 1 \sim 6$) denotes the eigenstate which corresponds to the n -th energy band. We can define the spin-orbital texture when $\lambda_{SO} \neq 0$ and $\Delta_{is} \neq 0$ because the finite values of λ_{SO} and Δ_{is} lift spin degeneracy. In addition, owing to the crystal symmetry which is described by the point group C_{4v} and the time-reversal symmetry, which is similar to the single orbital model, $\langle \hat{S}_z \rangle_{n,\mathbf{k}}$ and $\langle \hat{L}_z \rangle_{n,\mathbf{k}}$ become zero in the normal state. Hence, we can consider the in-plane spin (orbital) texture in the normal state through the direction of the spin

(orbital) polarization in xy -plane $\theta_S^{(n)}(\mathbf{k})$ ($\theta_L^{(n)}(\mathbf{k})$),

$$\theta_S^{(n)}(\mathbf{k}) = \arg[\langle \hat{S}_x \rangle_{n,\mathbf{k}} + i \langle \hat{S}_y \rangle_{n,\mathbf{k}}], \quad (36)$$

$$\theta_L^{(n)}(\mathbf{k}) = \arg[\langle \hat{L}_x \rangle_{n,\mathbf{k}} + i \langle \hat{L}_y \rangle_{n,\mathbf{k}}]. \quad (37)$$

Moreover, we define the direction of the momentum \mathbf{k} as $\theta_{\mathbf{k}} = \arg[k_x + ik_y]$.

In the superconducting state, we focus on the spin texture projected onto the electron space in the first excited state. We define the electron component of the spin operator in the three-orbital model as $\tilde{S}_{i=x,y,z}^e$ as

$$\tilde{S}_i^e = \frac{1}{2}[1 + \hat{\tau}_3] \otimes \hat{S}_i \otimes \hat{L}_0, \quad (38)$$

where \hat{L}_0 is the unit matrix in orbital space. We then introduce the angle $\theta_S^{SC1}(\mathbf{k})$ representing the direction of the spin operator in the xy -plane as

$$\theta_S^{SC1}(\mathbf{k}) = \arg[\langle \Psi_1(\mathbf{k}) | \tilde{S}_x^e | \Psi_1(\mathbf{k}) \rangle + i \langle \Psi_1(\mathbf{k}) | \tilde{S}_y^e | \Psi_1(\mathbf{k}) \rangle],$$

where $|\Psi_1(\mathbf{k})\rangle$ is the eigenstate of the first excited state in the BdG Hamiltonian.

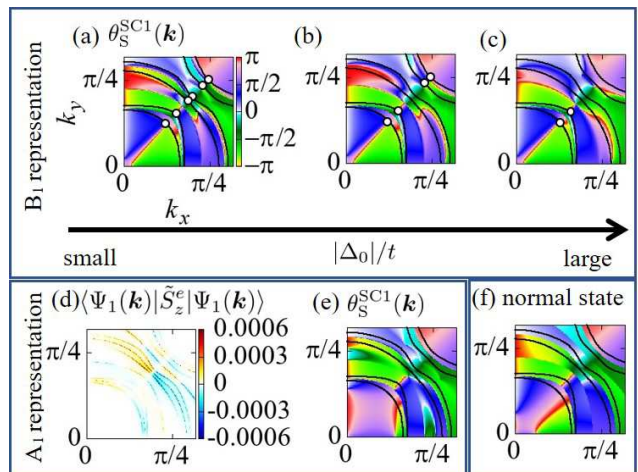


FIG. 1. The direction of the electron component of the spin polarization in the superconducting state for (a)(b)(c) B_1 and (e) A_1 pairing representations in the three-orbital model. The z -component of expectation value of spin in the three-orbital model for the A_1 representation is reported in (d). We set the gap amplitude $|\Delta_0|/t = 1.0 \times 10^{-3}$ for (a) and (e), $|\Delta_0|/t = 4.0 \times 10^{-2}$ for (b), and $|\Delta_0|/t = 0.10$ for (c). (f) The direction of the spin texture corresponding to the first excited state in the normal state with $\lambda_{SO}/t = 0.10$ and $\Delta_{is}/t = 0.20$.

In Figs. 1 (a), (b) and (c), we show how the electron component of the spin polarization pattern evolves by tuning the number of point nodes through a variation of the chemical potential for the superconducting configuration belonging to the B_1 representation. In Fig. 1 (e), the spin texture does not exhibit a topological structure. We can compare these spin textures with those of the normal state in Fig. 1 (f). Fig. 1 (d) is the z -component

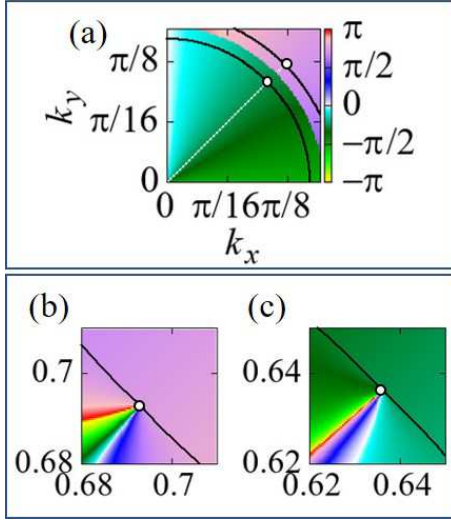


FIG. 2. The direction of the spin texture projected onto the electron space in the superconducting state in the single band model (a) with \mathbf{g} and \mathbf{d}_{3B_1} -vectors and (b)(c) with \mathbf{g} , \mathbf{g}_3 , \mathbf{g}_5 , \mathbf{d}_{1B_1} , and \mathbf{d}_{3B_1} -vectors at $\Lambda_R = 8.0 \times 10^{-2}$, and $|\Delta_0|/t = 1.0 \times 10^{-3}$. Black dotted line is Fermi surface at (a) $\mu/t = -0.25$ and (b)(c) $\mu/t = 0.35$. (b)((c)) is a magnified view around the point node on the outer (inner) Fermi surface. We set the parameters at $\Lambda_{3R} = \Lambda_{5R} = 0.0$, $r_s = 0.0$, and $f = 1.0$ for (a) and $\Lambda_{3R} = 0.70$, $a_1 = 1.0$, $a_2 = -1.0$, $\Lambda_{5R} = 1.0$, and $f = 0.99$ for (b) and (c).

of expectation values of spin in the three-orbital model for the A_1 representation. It becomes nonzero in the BZ owing to the spin-triplet/orbital-singlet ($d_{yz} \uparrow, d_{zx} \downarrow$) s -wave pairing. Hence, one can define the topological spin winding texture for the A_1 representation only by specifying the axis with respect to which the spin is winding. On the other hand, we can uniquely define the in-plane spin winding in the effective single orbital model because both of \mathbf{d} -vector and \mathbf{g} -vector lies on xy -plane as shown in Sect. II.

IV. SINGLE ORBITAL MODEL WITH HIGHER ORDER \mathbf{g} -VECTOR AND \mathbf{d} -VECTOR WITH B_1 SYMMETRY

In this section, we demonstrate the consequences of higher order \mathbf{g} and \mathbf{d} -vectors in the single orbital model and compare the obtained spin polarization pattern with the spin texture arising in the three-orbital model. We adopt the third and fifth order \mathbf{g} -vectors \mathbf{g}_3 and \mathbf{g}_5 , and the third order \mathbf{d} -vector for the B_1 representation \mathbf{d}_{3B_1} . Then the BdG Hamiltonian in the single orbital model is given by

$$\begin{aligned} \hat{H}_{\text{BdG}}(\mathbf{k}) = & \varepsilon(\mathbf{k})\hat{\sigma}_0 \\ & + [\Lambda_R \mathbf{g}(\mathbf{k}) + \Lambda_{3R} \mathbf{g}_3(\mathbf{k}) + \Lambda_{5R} \mathbf{g}_5(\mathbf{k})] \cdot \hat{\boldsymbol{\sigma}} \\ & + i\hat{\sigma}_y \hat{\boldsymbol{\sigma}} \cdot [(1-f)\mathbf{d}_{B_1}(\mathbf{k}) + f\mathbf{d}_{3B_1}(\mathbf{k})], \end{aligned} \quad (39)$$

and \mathbf{g} -vectors and \mathbf{d} -vectors are defined as

$$\begin{aligned} \mathbf{g}(\mathbf{k}) &= (\sin k_y, -\sin k_x, 0), \\ \mathbf{g}_3(\mathbf{k}) &= \mathbf{g}_3^{(1)}(\mathbf{k}) + \mathbf{g}_3^{(2)}(\mathbf{k}), \\ \mathbf{g}_3^{(1)}(\mathbf{k}) &= a_1((1 - \cos k_x) \sin k_y, -(1 - \cos k_y) \sin k_x, 0), \\ \mathbf{g}_3^{(2)}(\mathbf{k}) &= a_2((1 - \cos k_y) \sin k_y, -(1 - \cos k_x) \sin k_x, 0), \\ \mathbf{g}_5(\mathbf{k}) &= (\cos k_x - \cos k_y) \\ & \quad \times ((\cos k_x - 1) \sin k_y, (\cos k_y - 1) \sin k_x, 0), \\ \mathbf{d}_{B_1}(\mathbf{k}) &= |\Delta_0|(\sin k_y, \sin k_x, 0), \\ \mathbf{d}_{3B_1}(\mathbf{k}) &= |\Delta_0|(\cos k_x - \cos k_y)\mathbf{g}. \end{aligned}$$

Here, we neglect z -components of \mathbf{d} -vector and \mathbf{g} -vector since we are considering the C_{4v} point group.

Fig. 2 (a) reports the angular dependence of the electron component of the spin polarization for the first excited state of the superconducting spectrum in the single band model assuming \mathbf{g} and \mathbf{d}_{3B_1} -vectors. Here, we cannot define the spin polarization for the hole-like branch of the excited state due to $\mathbf{d}_{3B_1} = (0, 0, 0)$ in the diagonal direction. In addition, the spin orientation for the hole-like band has the same direction as that for the electron-like band because \mathbf{d}_{3B_1} -vector is parallel to \mathbf{g} -vector in the BZ. In Figs 2 (b) and (c), we show explicitly the resulting spin texture pattern in the superconducting state with \mathbf{g} , \mathbf{g}_3 , \mathbf{g}_5 , \mathbf{d}_{1B_1} , and \mathbf{d}_{3B_1} -vectors. In these figures, we set the ratio of \mathbf{d}_{B_1} and \mathbf{d}_{3B_1} -vector as $f = 0.99$. The result indicates that the spin polarization winds around the point node only when f is not equal to 1.

¹ G. Khalsa, B. Lee, and A. H. MacDonald, Phys. Rev. B **88**, 041302(R) (2013).

² Y. Fukaya, S. Tamura, K. Yada, Y. Tanaka, P. Gentile, and M. Cuoco, Phys. Rev. B **97**, 174522 (2018).